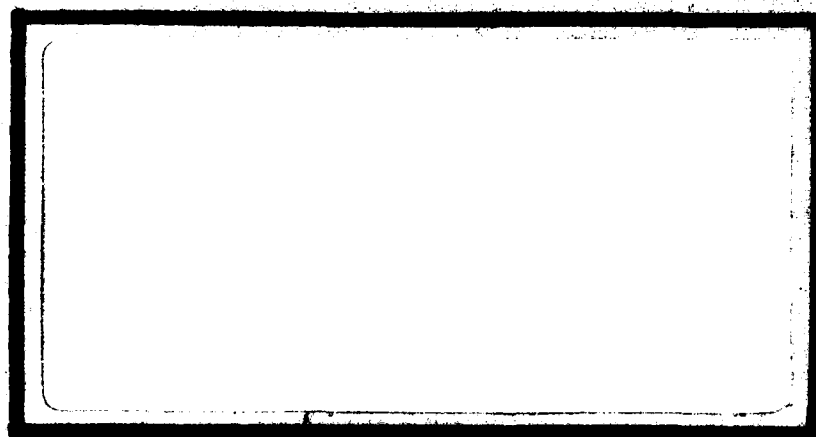|						
‖‖‖ **1.0**	4.5	**2.8**	**2.5**			
	5.0	**3.2**	**2.2**			
	5.6	**3.6**				
		4.0	**2.0**			
‖‖‖ **1.1**						
			1.8			
‖‖‖ **1.25**	‖‖‖ **1.4**	‖‖‖ **1.6**				

MICROCOPY RESOLUTION TEST CHART

NATIONAL BUREAU OF STANDARDS-1963-A

AD A124768

DTIC
SELECTED
FEB 2 2 1983
E

DEPARTMENT OF THE AIR FORCE
AIR UNIVERSITY (ATC)

AIR FORCE INSTITUTE OF TECHNOLOGY

Wright-Patterson Air Force Base, Ohio

83 02 022124

Optimization of a

He-Xe Hollow Cathode Discharge Laser

Thesis

AFIT/GEP/PH/82D-18   Jimmy C. Mann

Capt   USAF

DTIC
SELECTED
FEB 1983

E

OPTIMIZATION OF A

He-Xe HOLLOW CATHODE DISCHARGE LASER

THESIS

Presented to the Faculty of the School of Engineering

of the Air Force Institute of Technology

Air University

in Partial Fulfillment of the

Requirements for the Degree of

Master of Science

Accession For	
NTIS GRA&I	☒
DTIC TAB	☐
Unannounced	☐
Justification	

By	
Distribution/	
Availability Codes	
Dist	Avail and/or Special
A	

by

Jimmy C. Mann, B.S.

Capt   USAF

Graduate Engineering Physics

December 1982

Acknowledgements

I would like to acknowledge the guidance and assistance of Mr. Charles DeJoseph who provided the impetus for this thesis, and without whose help, completion would have been very difficult. He taught me the laboratory techniques needed for this experiment, patiently endured the numerous questions, and saved me countless hours of frustrations by pointing me in correct directions. My appreciation also goes to my faculty advisor, Lt. Col. Bailey, who offered me advise and then gave me free reign to learn as I conducted the experiment. Finally, I would be terribly remiss not to mention the loving support and understanding of my wife, Virginia.

J.C. Mann

Table of Contents

List of Abbreviations

Abbreviation	Meaning
a	variable = $-\ln[(1-Li)(1-T)]$
AFWAL	Air Force Wright Aeronautical Laboratories
BB	black body
dv	detector volts
f	focal length
g	dimensionless gain in laser cavity
HCD	Hollow Cathode Discharge
He	Helium
Hg	Mercury
Is	saturation intensity
j	current density
k'	complex propagation constant
ℓ	cavity length
L	total loss in the laser cavity
Li	internal loss in laser cavity
Ne	Neon
NEC	non-equal current (mode)
Po	power out
Pe	power emitted
Ps	power emitted by spontaneous emission at threshold
R	reflectivity
RMS	root mean square
T	transmittance

Ta	added transmittance
TEM	transverse electromagnetic mode
TGS	tri-glycerine sulfide
V	voltage
V-I	voltage vs current
Xe	Xenon
μm	micrometers (10^{-6}m) or microns
ρ	charge density (ro)

List of Figures

List of Tables

Abstract

This work investigates the characteristics of a fixed geometry hollow cathode discharge laser containing various pressures and mixtures of helium (He) and xenon (Xe). The laser oscillates at an infrared wavelength of 3.507 μm. Power from three output couplers using mixtures of 2.5% to 20% Xe at pressures of two to eight torr are investigated. The output power is measured as a function of mixture, pressure, and output coupler.

A "modes of operation" model is developed to explain the variations in the curves for power $\underline{vs}$ anode current. The symmetric mode of operation is characterized by equivalent voltages driving the three anodes at the same current. The asymmetric mode of operation is characterized by the same currents being driven by different voltages, hence the asymmetry. The non-equal current (NEC) mode of operation is characterized by at least one of the anodes being driven at a different current.

The results of the investigation reveal a maximum power of 1.16 mw with 10% Xe at 4 torr of pressure with an anode current of 27 mamps. Evidence is also presented that the asymmetric and NEC modes of operation can provide additional power after the symmetric mode has saturated.

I INTRODUCTION

The hollow cathode discharge is a compact and simple approach to electric gas discharge lasers because of the definite non-maxwellian nature of electron distribution and the high electron and ion densities achieved. The Air Force Wright Aeronautical Laboratories (AFWAL) at Wright-Patterson Air Force Base, Ohio, have developed a three anode, tubular, hollow cathode laser using a mixture of helium (He) and xenon (Xe) as the discharge medium. This continuous wave laser operates at an infrared wavelength of 3.507 μm. This wavelength is close to the stretching frequency of the carbon-hydrogen bond. Because of this fact, this laser may be useful as a probe laser for detecting hydrocarbons in the atmosphere and as a comustion diagnostic in the design of turbine engines.

The purpose of this experiment is to optimize this He-Xe hollow cathode discharge (HCD) laser with respect to gas mixture, gas pressure, discharge current, and output coupler.

For a better understanding of the principles involved in a hollow cathode discharge laser, the concepts of the glow discharge, the hollow cathode discharge, and the He-Xe hollow cathode laser of this experiment will be presented before the experiment is described.

The Glow Discharge

Gas discharges are achieved by applying voltage to electrodes within a gas. Figure 1 illustrates the V-I characteristics of gaseous discharges from 0.1 to 10 torr Hg (Ref 11:123).

The glow discharge is most commonly used in lasers because it is characterized by an essentially constant potential difference between

1
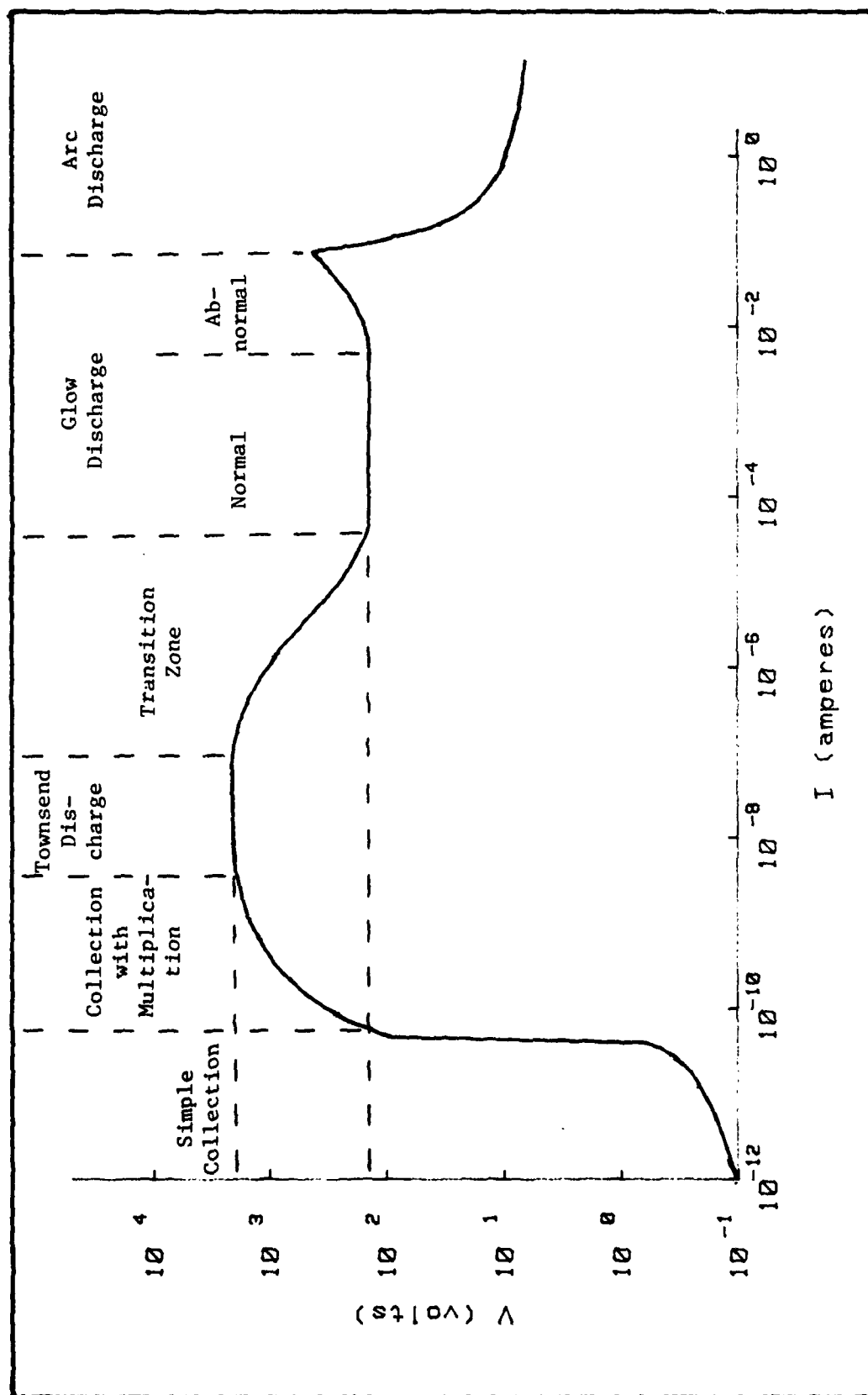
Figure 1. V-I Characteristics of a Gas Discharge

2

the electrodes over a wide range of currents. In contrast, the Townsend discharge does not have the electron number density for efficient excitation rates for a laser medium and the arc discharge does not access enough of the laser medium (Ref 18:30). In the arc discharge, the temperature of the gas approaches the temperature of the electrons and the population inversion necessary for a laser is usually lacking.

Figure 2 illustrates the diffuse luminous zones in a glow discharge, along with plots of the luminous intensity, electric potential, electric field, charge densities, and current densities. The zones will be briefly discussed in order from the cathode to the anode. The Aston's dark space is a result of secondary electrons ejected from the cathode by ion impact. These electrons do not have enough energy to ionize or excite the atoms of the gas and the ions have a small probability of recombination because of their velocity. Hence, this region does not emit any radiation. The cathode sheath appears at the point where ions or neutrals excited by electrons return to their ground level. In the Crookes (or cathode) dark space, the gas is ionized by the accelerated electrons which have not lost any energy exciting atoms passing through the cathode sheath, resulting in the large charge densities ($\rho+$ and $\rho-$) in this region. At pressures greater than about 1 torr, most of the electron energy is dissipated in the negative glow region of the discharge (Ref 17:460). In the Faraday dark space, the field is so small that the electrons cannot regain enough energy to excite or ionize the gas atoms. The positive column is the most luminous part of the discharge after the negative glow. It is characterized by a low electric field strength with slow electrons and small
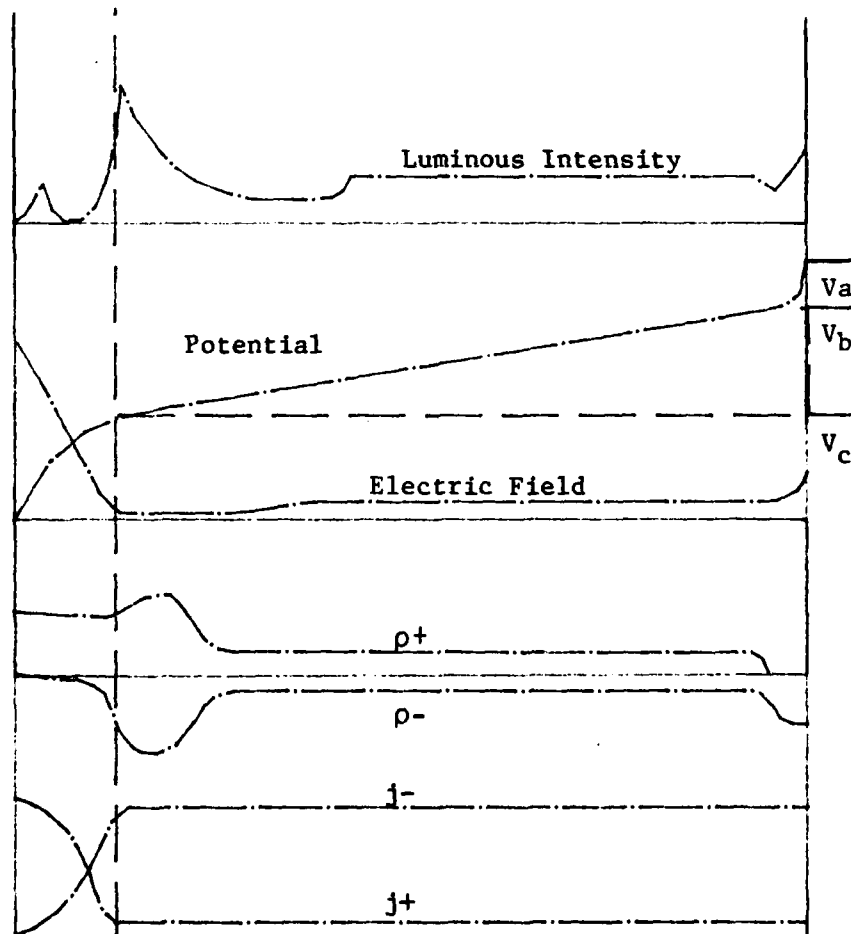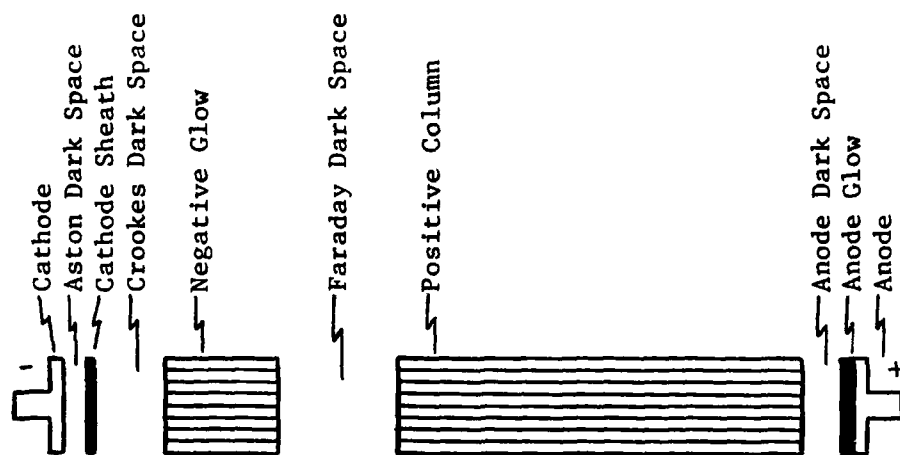
Figure 2.   Schematic of Glow Discharge Zones

excitation energy (Ref 11:130-132).

The proportions of these zones vary with pressure and the distance between electrodes. As the pressure decreases, the negative glow and the Faraday dark space expand at the expense of the positive column which diminishes and may even disappear. Decreasing the distance between the electrodes decreases the size of the positive column without varying the size of the other zones. Thus, the parts of the discharge near the cathode and the Crookes dark space are essential for maintaining the discharge. The positive column, however, is not (Ref 10:43).

The Hollow Cathode Discharge

One specialized form of gas discharge is the hollow cathode discharge (HCD). In its simplest form, figure 3a, the HCD consists of an anode and two plane cathodes (Ref 18:5). Each cathode has the various zones of the glow discharge. If the anode-cathode distance is decreased (at a constant pressure) the positive column will decrease until it disappears completely. If the distance separating the cathodes is then decreased, the negative glows of the two cathodes merge (figure 3b) and current densities increase for a constant voltage. Thus, the discharge efficiency (current density/voltage) is increased. For small pressures, the current densities can be 10^2 to 10^3 higher than the normal cathode current densities (Ref 19:236). Figure 3b illustrates the merged negative glows with a "split rod" configuration. If the cathode is shaped into an almost circular shape, the geometry results in the circular negative glow of the HCD in this experiment. (See figure 3c.)

The electron-energy distribution in a HCD is due to multiple ionization and excitation processes. In the positive column, electrons are
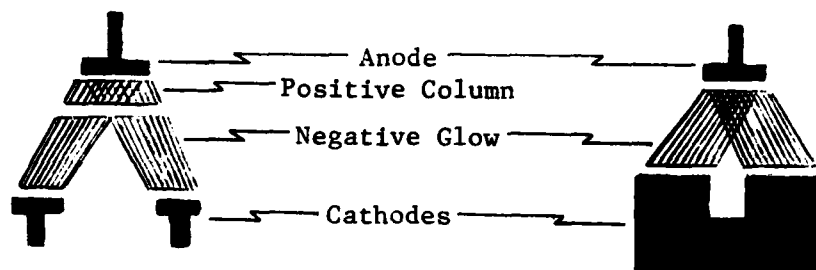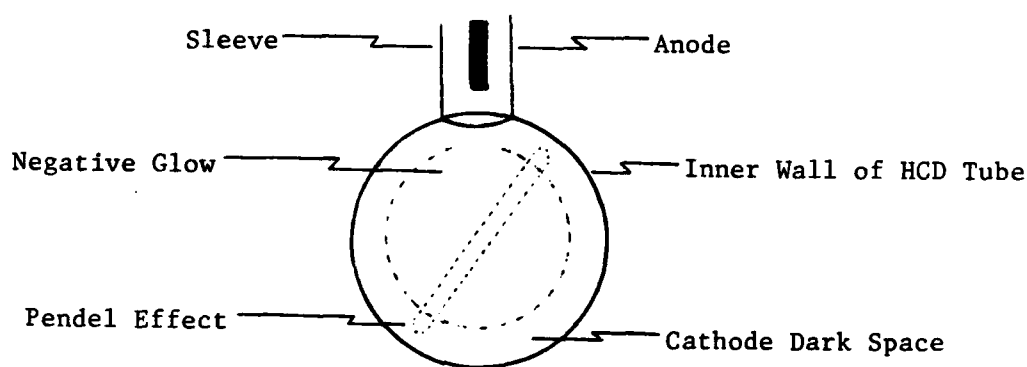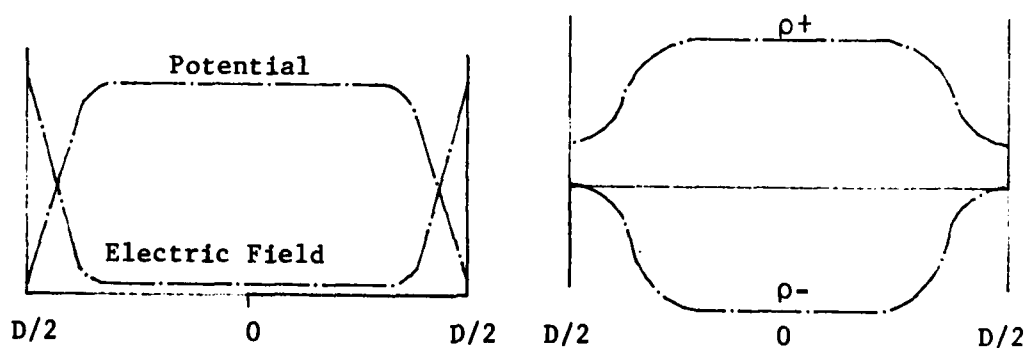
Figure 3. Hollow Cathode Discharge Development

accelerated by the electric field. Since the field in the HCD is much weaker, however, other processes must account for the increased current density and subsequently higher discharge efficiency. In the hollow cathode discharge tube, the cathode is the circular shaped section of the tube. The symmetry of this arrangement enhances ionization through the Pendel effect and through increased secondary emission by non-charged particles (Ref 17:460-461).

The Pendel effect is illustrated in figure 3c (Ref 18:7). Electrons are emitted into the gas discharge from the cathode. Because of the HCD geometry, any electron passing through the discharge enters the opposite cathode dark space, is repelled by the high field, and re-enters the negative glow. Thus, the electrons oscillate from side to side within the negative glow. Ionization is enhanced as the electrons deposit their energy into the negative glow rather than a less efficient positive column (Ref 18:6).

In the positive column, a significant fraction of the noncharged particles which might have created secondary emissions by collision with the cathode are lost to the walls or to the anode because they are unaffected by the field. In the HCD geometry, however, an increased proportion of these particles strike the surrounding cathode and the total secondary emission efficiency of the discharge rises (Ref 17:461). The increase in electron density further enhances ionization of the gas.

Helium and Xenon Hollow Cathode Discharge Laser

The He-Xe hollow cathode discharge laser in this experiment oscillates in an atmospheric window at 3.507 μm. The atmospheric transmittance due to molecular absorption of 3.51 μm through a 10 km

horizontal path is 0.91 at sea level and 1.00 at 12 km elevation (Ref 9:116).

The specific Xe laser transition is from the $5d[3\frac{1}{2}]_3^0$ state to the $6p[2\frac{1}{2}]_2$ state (Ref 8:299). This notation is the Racah notation (Ref 15:537).

Earlier investigations of Xe have shown it to be a very high gain medium. Heavens investigated the oscillation of Xe (9% at 2 torr) at eleven wavelengths from 2.0261 μm to 5.5738 μm and recorded "the remarkably high gain of 120 percent per meter compared to 2-12 percent for the He-Ne lines (Ref 6:70)." Lengyel used 0.1% Xe at 2 torr in a 5-7 mm diameter tube and achieved 1 percent per cm at 2.0262 μm and 13 percent per cm at 3.507 μm (Ref 8:205).

Another advantage of the Xe lasers has been the small width of their emission line (Ref 12:115). The normally narrow laser line is not significantly affected by doppler broadening because of the larg, mass of the Xe atoms (Ref 10:768).

Unlike the He-Ne laser, though, there is no energy transfer between helium and xenon (Ref 8:205). The function of helium is probably to increase the density of free electrons (Refs 8:205; and 16:511) thereby increase the efficiency of excitation (Ref 12:115).

II EXPERIMENTAL PROCESS

Scope

This section describes the experimental apparatus and techniques used in this experiment. The experimental appratus section is divided into five functional groups: discharge tube; laser cavity; vacuum and gas supply systems; high voltage electrical system; and the optical detecting system. The experimental techniques discussion outlines the system evacuation and filling procedures and the power measurement procedures. A section on radiometry briefly describes the calibration of the pyroelectric detector.

Experimental Apparatus

Discharge Tube. The hollow cathode discharge tube shown in figure 4 is constructed from 3/8 inch O.D. 304 stainless steel tube with 0.070-inch wall thickness. The tube length is 8.5 inches with three anodes 2.25 inches apart and 2 inches from either end. The anodes are constructed from 304 stainless steel with ends recessed 0.240 inches from the inside diameter of the discharge tube. To prevent the anode from shorting to the cathode, a 0.035-inch thick alumina sleeve around the anode extends to the inside diameter of the discharge tube. A ceramic adhesive insulates and seals the anode (Ref 18:12). The temperature of the discharge tube was monitored by a K-type thermocouple connected to a Fluke 8024A Digital Multimeter.

A mini-conflat flange is welded to each end of the discharge tube. These flanges are connected to mated flanges with calcium fluoride brewster windows. A third flange is welded between the first anode and the tube end. It is mated to a flange with a bellows valve connecting
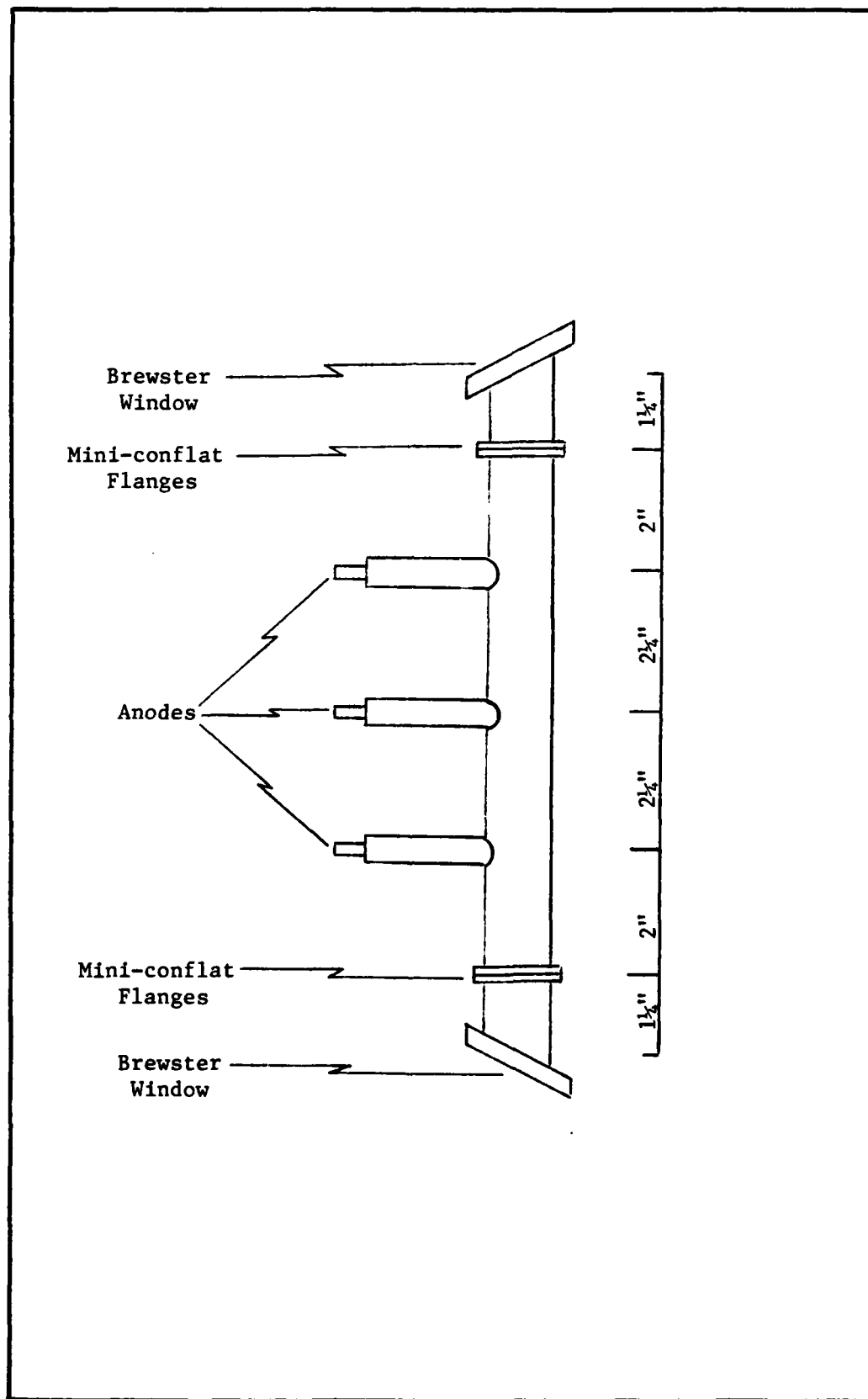
Figure 4. He-Xe Hollow Cathode Discharge Tube

Brewster
Window

Mini-conflat
Flanges

Anodes

Mini-conflat
Flanges

Brewster
Window

$1\frac{1}{2}''$ $2''$ $2\frac{1}{4}''$ $2\frac{1}{4}''$ $2''$ $1\frac{1}{2}''$

10

the vacuum and gas supply system. A wire mesh screen with stainless steel wires every 1.0mm is inserted in the side arm containing the bellows valve.

Laser Cavity. The laser cavity is composed of two mirrors mounted at a fixed distance of 32.53 cm. No attempt is made to vary this distance since the object of the experiment is to derive the optimum mixture and pressure for the medium within the hollow cathode discharge. The cavity mirrors are mounted with very stable and precise micrometer adjustments. Both mirrors are made of germanium, but with different transmission coatings. The aft mirror is a total reflector (R > 99%). The output coupler is varied using three couplers: coupler #1 (R = 89.5%); coupler #2 (R = 79.0%); and coupler #3 (R = 95.6%).

Vacuum and Gas Supply System. The gas handling system is shown in figure 5. Stainless steel vacuum lines and fittings are used with copper gaskets at all couplings. The pump for the roughing system evacuates the system to about 30 microns of pressure. The Granville-Phillips Series 205 diffusion pump with liquid nitrogen cold trap evacuates the system to a high vacuum; typically, 10^{-6} torr.

The absolute pressure within the system is measured with one of two gauges. The 10-torr head (145 BHS-10) to the MKS Varatron is used to measure the pressures for the roughing system and for the gas mixtures. For low pressure evacuation with the diffusion pump, a Varian "nude" Baird-Alpert ionization gauge is used. To enhance equipment lifetime, the 1% emission rate of the ionization gauge was used. The 1% emission rate is sufficient since the experiment calls for gas mixtures of one to eight torr of pressure and the diffusion pump evacuates the system to about 10^{-6} torr.

11

Laser

Bellow Valves #1, 2   Butterfly Valves #3, 4

Gold Seal Valve #5   Toggle Valves #6, 7

Needle Metering Valves #8, 9

RP = Roughing Pump   DP = Diffusion Pump

TG = Thermouple Gauge   IG = Ion Gauge

BG = MKS Baratron Gauge
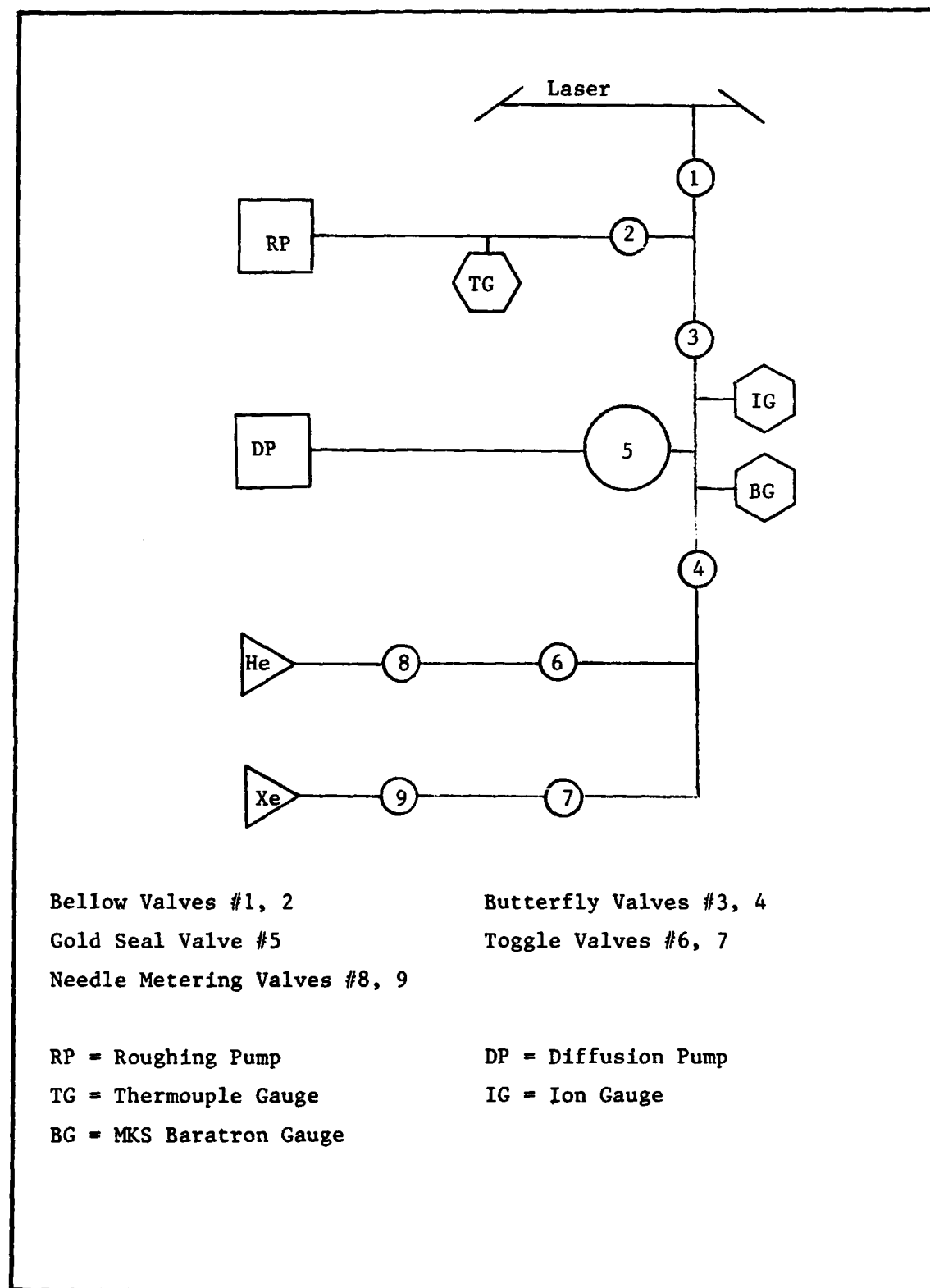
Figure 5. Vacuum and Gas Supply System

12

The He and Xe lines each have a toggle valve for positive cutoff and a needle metering valve for precision metering.

High Voltage Electrical System. The high voltage electrical system is shown in figure 6. High voltage is supplied by a Gregory-King Electronics 3kv 1A DC unregulated power supply. It is typically operated at 1kv to feed power into a 10-channel current regulator which was built in-house.

In this experiment, only three of the ten channels of the current regulator are used at one time. The current regulation for each channel is controlled by a 10-turn potentiometer. In order to guarantee maximum agreement in current settings, each potentiometer used was slipped until the currents of the channels used were within 0.17 mamps of each other (verified at 3, 8, 16, and 24 mamps). The potentiometers are connected by a non-slip drive belt. The output of each channel is connected to an anode of the hollow cathode discharge tube.

The median current is run through an ammeter and then to the second (middle) anode of the hollow cathode discharge tube. The discharge voltage is measured with the high voltage probe and digital voltmeter combination. The high voltage probe is connected to the middle anode for most of the experiment, but is temporarily held to the first and third anodes when comparative voltage readings are required for mode determination.

Optical Detection System. The optical detection system is shown in figure 7. The beam is chopped by a rotary chopper and then focused by an arsenic trisulfide lens (f = 6.1 cm at 3.51 μm) to a triglycine sulfate (TGS) pyroelectric detector from Laser Precision Corp. The output of the detector is amplified and fed into a Fluke

13
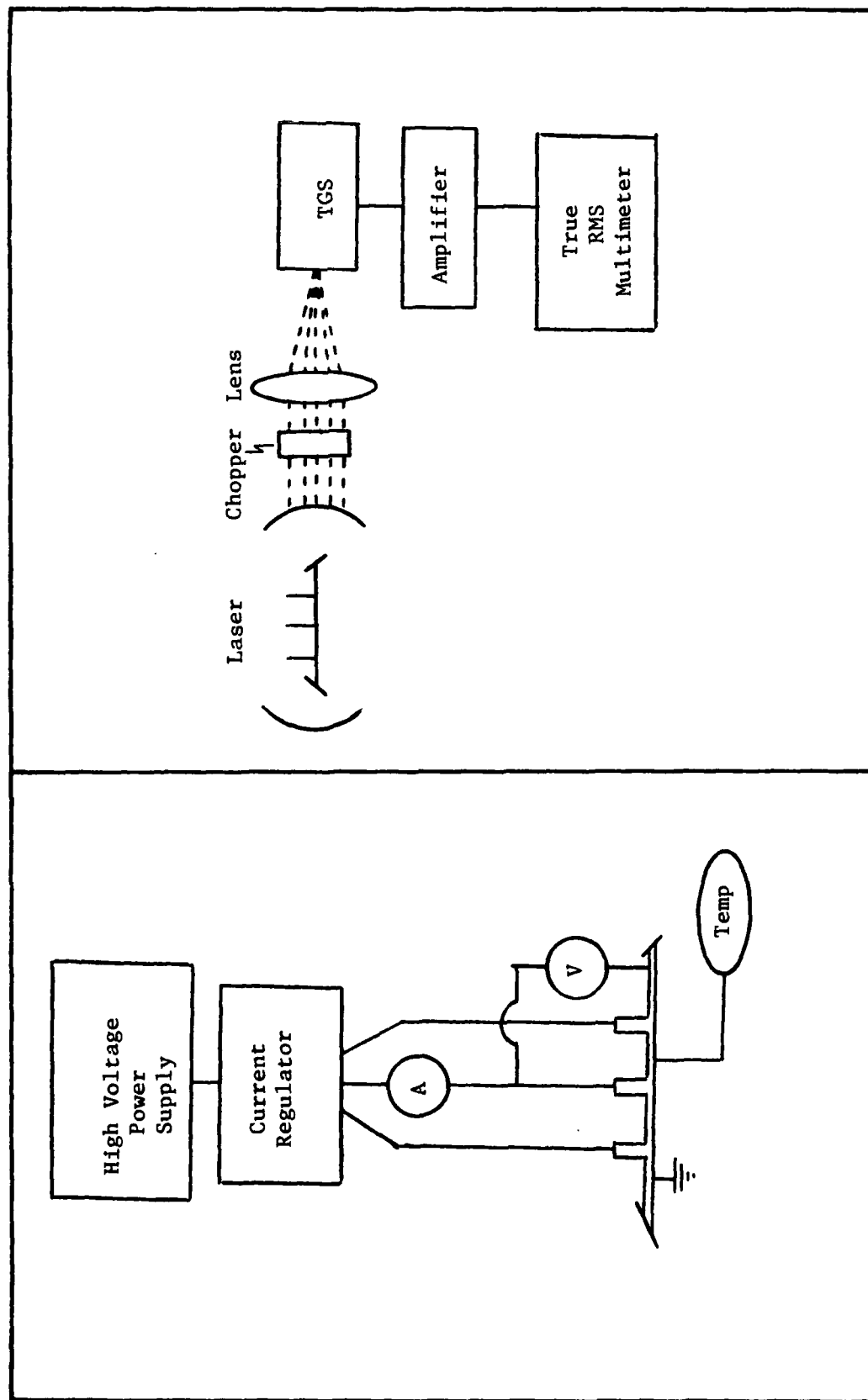
Figure 7. Schematic of Optical Detection System for Power Measurement

Figure 6. High Voltage Supply System

14

8050A Digital Multimeter with true RMS readout.

Experimental Techniques

Evacuation and Filling. To enhance outgassing during evacuation, the hollow cathode is heated by running a discharge at high current until the temperature readout is 55-60°C. After the power is turned off and the voltage of the power source is back to zero, valves #1 and #2 (figure 5) are opened and the roughing pump evacuates the system to 30 microns of pressure. Then, valve #2 is closed, the gold seal valve (#5 in figure 5) is opened, and the diffusion pump with liquid nitrogen cold trap evacuates the system to high vacuum. The system is evacuated to a pressure of 3×10^{-6} torr or lower. Valve #5 is then closed, the ionization gauge is turned off, and butterfly valve #3 is closed. Thus, a pre-mix chamber is established between the gas lines and valve #3.

Gases are mixed by the method of partial pressures. For example, toggle valve #7 and metering valve #9 are opened until 0.499 torr of Xe fills the pre-mix chamber. Valves #7 and #9 are then closed and the procedure is repeated with the He valves (#6 and #8) until the MKS Baratron indicates a total of 4.990 torr of pressure. After valves #6 and #8 are closed, valve #3 is opened and the 10% mixture of Xe is turbulently mixed as it fills the evacuated portion of the system between valve #3 and the discharge tube. The pressure gauge then indicates a total pressure in the entire system of 4.000 torr. (The ratio of entire system to pre-mix chamber is 1.273.)

Various pressures of the same gas mixture are obtained by mixing the gases at the highest pressure required, taking the measurements, and then slowly opening valve #2 to the roughing system. The system

15

pressure is thus bled down to the desired pressure for the next run of measurements.

Power Measurements. Measurements of the laser power without the focusing lens proved perplexing because of great power fluctuations with very small movements of the laser mirrors or with changes of current. This extreme sensitivity was atypical of familiar laser systems. The beam was probably non-uniform and the adjustments of the mirror mounts for maximum voltage readout from the detector were actually the adjustment of "hot spots" within the beam onto the detector (Ref 5).

For a total power measurement of the beam, the chopped beam is focused onto the pyroelectric detector. The true RMS digital multimeter provides the detector volts (dv) used to record the output of the HCD laser.

At a given current setting, the power out also proved to be affected by the temperature of the hollow cathode and therefore by time. For consistency, the power out reading is accepted as the maximum quasi-stationary dv power reading within $3\frac{1}{2}$ minutes or by the time the hollow cathode reached 60°C, whichever comes first.

The anode voltages used for the efficiency comparisons are obtained from the high voltage probe on the middle anode, generally the median value of the three anodes.

Radiometry

The purpose of this experiment is to determine the relative output powers for various mixtures and gas pressures of the He-Xe HCD laser. For perspective, though, it is also important to relate the absolute power of this laser to other lasers. Thus, it is necessary to calibrate the detector.

16

The calibration of the pyroelectric detector was accomplished with a Model 11-200 High Temperature Infrared Radiation source from Barnes Engineering Co. as a black body (BB) standard.

Detectors generate a signal which is a function of both power and response (Ref 7:93). The generated signal is therefore the integral of the responsivity and power.

$$S = \int P(\lambda)\, R(\lambda)\, d\lambda \tag{1}$$

$$= \int A I_{BB}(\lambda)\, d\Omega\, R(\lambda)\, d\lambda \tag{2}$$

or $\quad S = A\Omega \int I_{BB}(\lambda)\, R(\lambda)\, d\lambda \tag{3}$

for a small detector at a large distance from the source.

One of the advantages of pyroelectric detectors is that they have a flat response because they respond to temperature changes due to power received. So, since temperature is energy dependent rather than wavelength dependent, pyroelectric detectors are generally independent of wavelength. Thus.

$$S = A\Omega \bar{R}\, \sigma T^4 \tag{4}$$

where σ is the Stephan-Boltzmann constant.

Thus, measuring the signal at a temperature T, of a source of area A, a distance r away, with a detector size A_d:

$$R = \frac{S\, r^2}{A\, A_d\, \sigma\, T^4} \tag{5}$$

The detector was calibrated at 500°, 600°, 700°, 800°, and 900°C. Applying the data to equation #5, the responsivity of this detector and rotary chopper combination is:

$$R = (5.444 \pm 0.046) \times 10^3 \text{ w/mv}$$

or $\quad R^{-1} = (1.837 \pm 0.016) \times 10^{-1}$ mw/v.

The small standard deviations over the large range of temperatures attests to the flat response of the pyroelectric detector. The validity of the calibration was further checked by a linearity check. The calibration had been accomplished with a black body aperture of 3.3×10^{-1} cm^2. The calibration was repeated at 900°C with five other apertures from 1.0×10^{-1} to 1.0×10^{-3} cm^2. The results had a standard deviation of less than five percent.

To determine the effective transmittance of the As$_2$S$_3$ lens at 3.51 μm, two more sets of calibrations were made. The first was made with a narrowband filter with half maximum values of 40% at 3.398 μm and 3.599 μm. The final set of calibrations was made with the lens and filter in place. Since a different solid angle is generated with the lens, it was necessary to know the diameter of the lens. However, the edges of the lens were non-uniform and probably less effective than the paraxial section used in the experiment. Therefore, a variable (iris) aperture with a set diameter of 1.62 cm was used in front of the lens. To ensure the proper focus, the black body radiation was focused with the 3.5 μm filter in place. An equivalent responsivity for each case was calculated at each temperature. The ratio of the averages resulted in an effective transmittance of 72.4% (at 3.51 μm) for the lens. Thus, for the entire system at 3.51 μm:

$$P = \frac{S}{0.724} \times (0.1837 \text{ mw/v})$$

or $\quad P = (0.254 \text{ mw/v}) \times S \qquad (6)$

III THEORY

Modes of Operation

As the experiment was conducted, many unexpected phenomena were encountered. High pressures had power dips. Low pressures had leveling and even declining curves. At times, small pressure changes caused disproportionate power changes. If the bellow valve at the hollow cathode was opened or closed, the physical discharge and the power out changed abruptly.

These phenomena appear to be the result of the transition of the discharge from one mode of symmetry operation to another. A symmetric mode of equivalent voltages driving the three anodes at the same current is the expected mode of operation. Under some conditions, though, an asymmetric mode evolves; a mode in which the same currents are maintained by different voltages at the anodes. This asymmetry is due in the most part to plasma "creep." The plasma actually leaves the axial portion of the hollow cathode tube and extends into the side arm of the vacuum system.

This extension of the plasma is probably due to the plasma seeking more surface area for primary electron emission, i.e., a larger cathode. The larger cathode results in a lower voltage driving the same current. This lower voltage on the first anode results in an "asymmetric" mode of operation; asymmetric because the voltages and glow discharges are now different. This asymmetry causes gradients within the hollow cathode discharge and destroys the uniformity of the plasma within the laser volume.

In order to present a potential barrier to the plasma, a wire

mesh screen was installed at the junction of the side arm of the hollow cathode. In spite of the screen, though, the plasma would still transition into an asymmetric mode of operation at some pressures and mixtures. It would appear that the wire screen merely reduced the number of transitions.

Although a uniform excitation of a long column is normally the accepted premise of hollow cathode discharge lasers (Ref 16:61), this non-uniformity is not necessarily an undesirable effect. When the power in the symmetric mode begins to level, the asymmetric mode of operation can actually generate more power from the laser. This aspect will be demonstrated in the power comparisons of section IV.

Gain and Loss Parameters

This treatment for gain and loss measurement relies heavily on chapter 6 of Yariv's book (Ref 21 and chapter 3 of Pedrotti's unpublished book (Ref 13).

The total outgoing wave of a laser is (Ref 21:114):

$$E_t = t_1 t_2 E_i e^{-ik'\ell} [1 + r_1 r_2 e^{-i2k'\ell} + r_1^2 r_2^2 e^{-i4k'\ell} + \cdots] \tag{7}$$

Figure 8, however, illustrates that if a known loss is inserted via an added transmittance, Ta, it scales with the exponential term.

$$E_t = t_1 t_2 Ta E_i e^{-ik'\ell} [1 + r_1 r_2 Ta^2 e^{-i2k'\ell} + r_1^2 r_2^2 Ta^4 e^{-i4k'\ell} + \cdots] \tag{8}$$

or

$$E_t = E_i \left[\frac{Ta t_1 t_2 e^{-ik'\ell}}{1 - Ta^2 r_1 r_2 e^{-i2k'\ell}} \right] \tag{9}$$

The oscillation requirement is that the denominator become zero, or

$$1 = Ta^2 r_1 r_2 e^{-i2k'\ell} \tag{10}$$

20
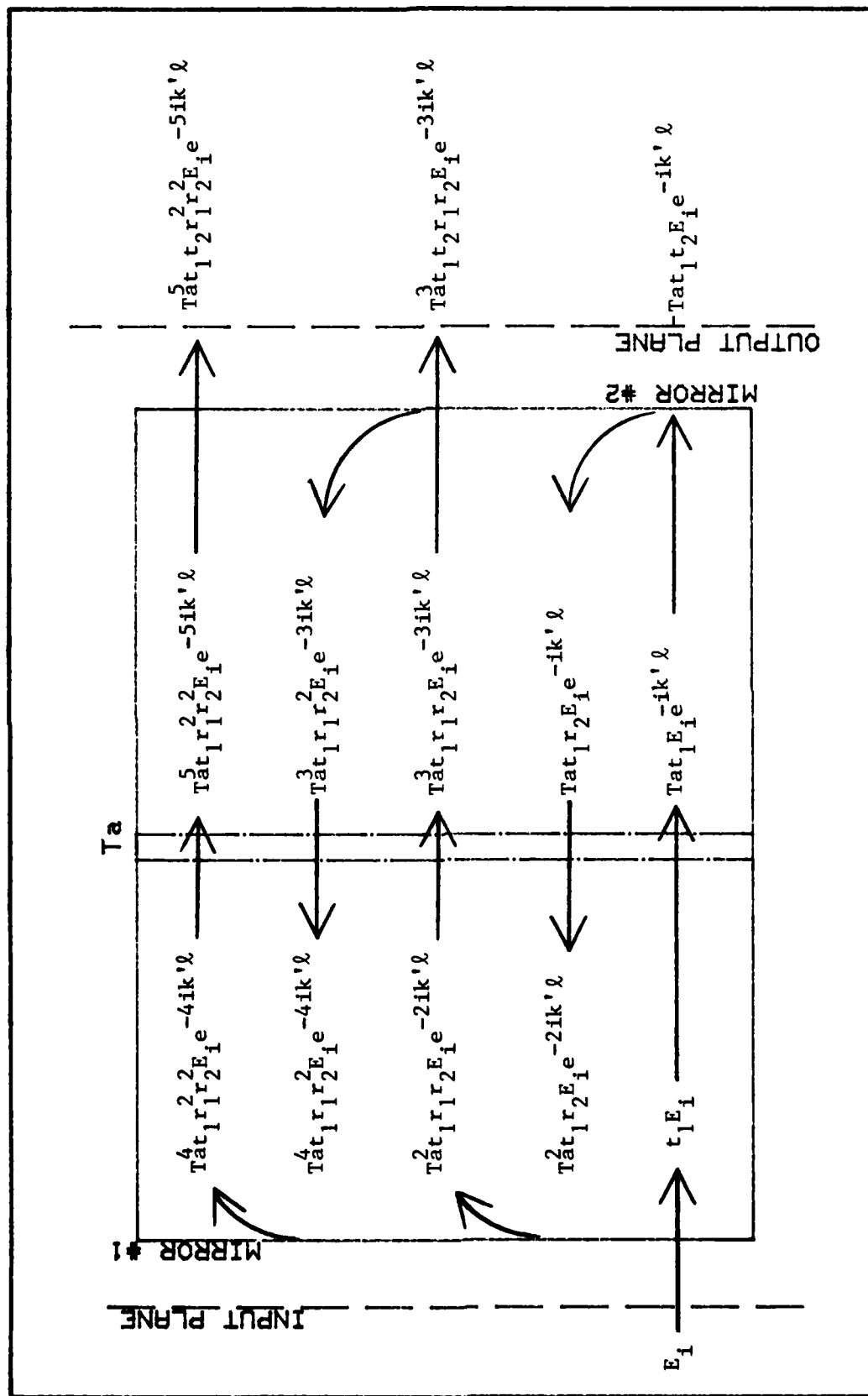
Figure 8. Model Used to Analyze a Laser Oscillator With an Inserted Loss (Added Transmittance)

OUTPUT PLANE

$Tat_1^5 t_2 r_1^2 r_2^2 E_i e^{-5ik'\ell}$

$Tat_1^3 t_2 r_1 r_2 E_i e^{-3ik'\ell}$

$Tat_1 t_2 E_i e^{-ik'\ell}$

MIRROR #2

$Tat_1^5 r_1^2 r_2^2 E_i e^{-5ik'\ell}$

$Tat_1^3 r_1 r_2^2 E_i e^{-3ik'\ell}$

$Tat_1^3 r_1 r_2 E_i e^{-3ik'\ell}$

$Tat_1 r_2 E_i e^{-ik'\ell}$

$Tat_1 E_i e^{-ik'\ell}$

Ta

$Tat_1^4 r_1^2 r_2^2 E_i e^{-4ik'\ell}$

$Tat_1^4 r_1 r_2^2 E_i e^{-4ik'\ell}$

$Tat_1^2 r_1 r_2 E_i e^{-2ik'\ell}$

$Tat_1^2 r_2 E_i e^{-2ik'\ell}$

$t_1 E_i$

MIRROR #1

INPUT PLANE

E_i

21

where r_1 = reflectivity of mirror 1

r_2 = reflectivity of mirror 2

and T_a = transmittance of added loss.

The amplitude portion of this complex k' thus requires:

$$1 = T_a^2 r_1 r_2 e^{\{\gamma_t(\omega) - \alpha\}\ell} \tag{11}$$

Hence,

$$\gamma_t(\omega) = \alpha - \frac{1}{\ell} \ln(T_a^2 r_1 r_2) \tag{12}$$

or

$$\gamma_t(\omega) = \alpha - \frac{1}{\ell} \ln(T_a^2 r_2) \tag{13}$$

for $r_1 = 1.00$.

However, the gain (Ref 21:125) is:

$$\gamma = \frac{\gamma_0 \ell}{1 + P_e/P_s} \tag{14}$$

where γ_0 = unsaturated gain coefficient

P_e = total emitted power

P_s = power emitted by spont, emission at threshold.

Once the oscillation threshold is exceeded, $\gamma = \gamma_t$.

Thus,

$$P_e = P_s \left\{ \frac{\gamma_0 \ell}{\alpha - \ln(T_a^2 r_2)} - 1 \right\} \tag{15}$$

However, the useful output of the laser is but a fraction of the emitted power, specifically, $[-\ln(1-T)]/L$

where

$$L = \alpha\ell - \ln(T_a^2 r_2) \tag{16}$$

representing the total losses of the system. Hence,

$$P_o = P_s \frac{-\ln(1-T)}{L} \left\{ \frac{\gamma_0 \ell}{L} - 1 \right\} \tag{17}$$

or, substituting the atomic parameters for the power emitted by spontaneous emission at threshold (Ref 21:126),

$$P_o = \left\{ \frac{8\pi n^3 h \Delta \nu V}{\lambda^3 t_c} \frac{t_{spont}}{t_2} \right\} \left\{ \frac{-\ln(1-T)}{L} \right\} \left\{ \frac{\gamma_0 \ell}{L} - 1 \right\} \tag{18}$$

but, $\quad t_c = \dfrac{n\ell}{Lc} \tag{19}$

and the output power becomes:

$$P_o = \left\{ \frac{8\pi n^2 h \Delta \nu V c}{\lambda^3 \ell (t_2/t_{spont})} \right\} \left\{ -\ln(1-T) \right\} \left\{ \frac{\gamma_0 \ell}{L} - 1 \right\} \tag{20}$$

This agrees with Pedrotti (Ref 13:3-43) and differs from Yariv only in the fact that the approximation $-\ln(1-T) \simeq T$ is not used. Note that this approximation would have been inappropriate in the case of (1-T)=R=0.790 for coupler #3 in this experiment. Let

$$(Is)A = \frac{8\pi n^2 h \Delta \nu V c}{\lambda^3 \ell (t_2/t_{spont})} \tag{21}$$

where $A = V/\ell$, the cross sectional area of the mode and (Is) is the saturation intensity (Ref 21:108).

Let

$$g = \gamma_0 \ell \tag{22}$$

and $e^{-\alpha \ell} = 1 - Li \tag{23}$

where Li represents the internal losses of the system including diffraction losses, scattering and absorption by imperfect Brewster windows, etc. (Ref 16:3-45). Finally:

23

$$P_o = (Is)A[-\ln(1-T)]\left[\frac{g}{-\ln[(1-Li)(1-T)]-\ln(Ta^2)} - 1\right] \qquad (24)$$

The optimum coupling is found by setting the derivative with respect to T equal to zero. Thus:

$$(1 - T_{opt}) = \exp[L - \sqrt{gL}]$$

or $\qquad R_{opt} = \exp[Li - \sqrt{gLi}] \qquad (25)$

$$\text{for } Ta = 1.00$$

A least squares fit of a number of data points to the non-linear equation:

$$P_o = C\left[\frac{g}{a + x} - 1\right] \qquad (26)$$

where $C = (Is)A[-\ln(1-T)] = $ constant $\qquad (27)$

$\qquad g = $ gain $\qquad\qquad\qquad\qquad\qquad\qquad\qquad (22)$

$\qquad a = -\ln[(1-Li)(1-T)] \qquad\qquad\qquad\qquad (28)$

and $\quad x = -\ln[Ta^2]$, the independent variable

will yield the desired gain of the medium as well as the internal loss, Li. Obviously, the more inserted losses used, the better the resolution of the parameters of the laser medium, provided, of course, that accuracy is within acceptable limits.

In fact, if the measurements are accurate, power out comparisons should be valid by changing the "T" values and obtaining a theoretical power figure. Within the medium, Li and g are not functions of T, but the oscillation condition is. From equation 27,

$$C = (Is)A[-\ln(1-T_M)] \qquad (28)$$

where T_M is the coupler used in the measurement.

For the jth coupler, Tj,

$$Cj = C \left[\frac{\ln(1-Tj)}{\ln(1-T_M)}\right] \tag{29}$$

Hence,

$$Pj = C \left[\frac{\ln(1-Tj)}{\ln(1-T_M)}\right]\left[\frac{g}{-\ln[(1-Li)(1-Tj)]} - 1\right] \tag{30}$$

Thus, a theoretical power out, Pj, can be compared to actual power out, Po, to verify the g and Li calculations.

Alternate Method. An alternate method is to insert high losses which will inhibit the oscillation of the laser until it approaches threshold. This method yields a linear approximation to the tail of the power curve and requires a mere linear regression instead of the more involved non-linear fit.

Unfortunately, the resultant figure is the value of the "net" or effective gain of the medium.

$$P_o = \left[\frac{g}{a + x} - 1\right] = 0$$

requires that x = g-a or that the x-intercept equal the gain minus the losses. If neither g nor Li is known, the other cannot be determined.

IV ANALYSIS AND DISCUSSION OF RESULTS

Modes of Operation

In this experiment, the hollow cathode discharge exhibited definite "modes of operation." For example, figure 9 illustrates the large difference in output with a pressure change of one torr. The broken line (4 torr) reveals a leveling trend of the power followed by an increase. The solid line (5 torr) depicts power out increasing in a more familiar manner.

A study was undertaken to determine what causes such a behavior in a small parameter change. In figure 10, the solid curve of 5 torr is duplicated, but the broken line labeled "MODIFIED" is much more linear in the 6-12 mamp region. Above 15 mamps (per electrode), the curves coincide. The difference lies in different modes of operation: symmetric vs asymmetric. The asymmetric mode is characterized by unequal voltages driving equivalent currents.

The modification which resulted in the broken line was to set the current, allow the power to stabilize (at the solid curve level), disconnect the second anode, and then reconnect the second anode. This modification will be referenced as the 3,2,3 modification. At the lower currents, no change was evident. Above 15 mamps, the mode of operation had already evolved into the asymmetric mode of operation. In the 6-12 mamp range, the anode voltages and power out changed. Typical figures are in Table I.

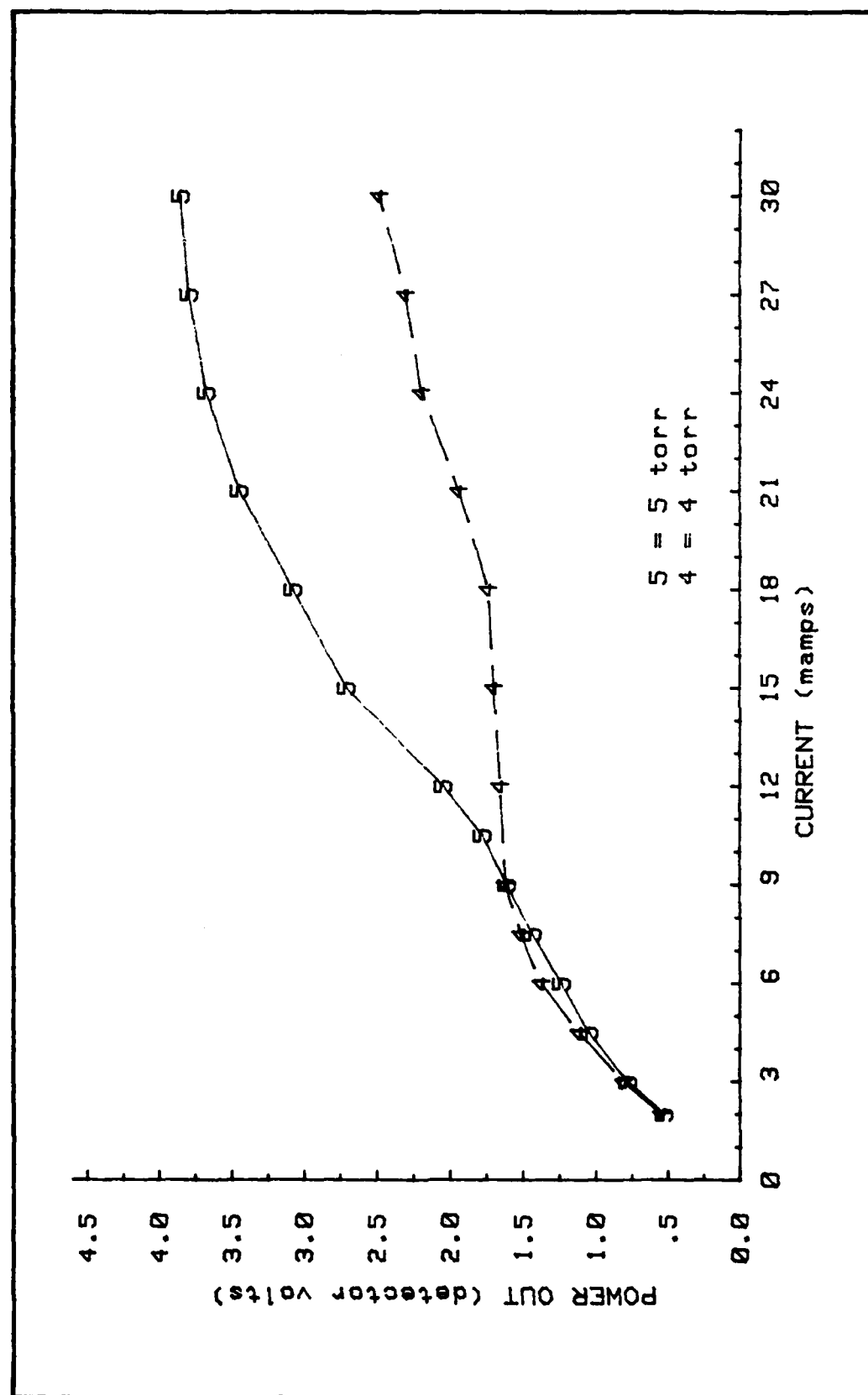Figure 9. Power Curves for 5% Xe at 5 torr and 4 torr

SOLID LINE = NATURAL MODE
BROKEN LINE = MODIFIED (3,2,3) MODE

CURRENT (mamps)
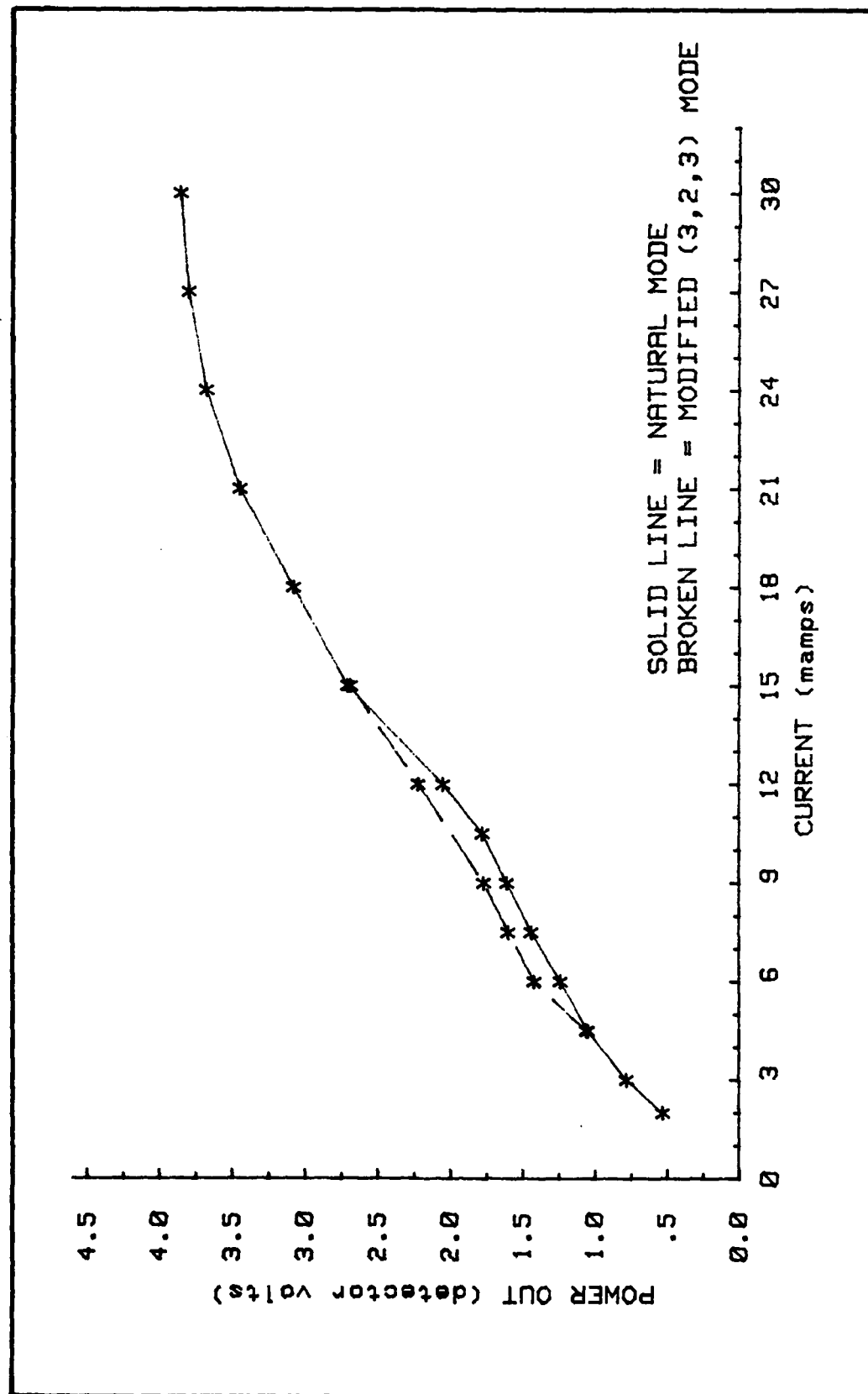
POWER OUT (detector volts)

Figure 10. Power Curves for 5% Xe at 5 torr in the Natural
and the Modified Modes of Operation

Table I

Power and Anode Voltage Comparison in Different
Modes of Operation With 5% Xe at 5 Torr

| ANODES | ANODE VOLTAGE | | | POWER OUT |
CONNECTED	#1	#2	#3	(detector volts)
1,2,3	320	325	327	1.96
1, 3	313	0	325	2.22
1,2,3	313	323	325	2.20

This example illustrates the difference between the symmetric (first case) and the asymmetric (last case) modes of operation.

An initial explanation would be that the gain is saturated with the full complement of three anodes. A brief investigation, though, of 5% Xe at 4 torr revealed the three curves in figure 11. The symmetric mode leveled off. Using only two anodes resulted in only slightly more power after the level off. However, the 3,2,3 modification increased power significantly* If the medium is saturated in the three anode condition, one would not expect the power to be significantly higher under the 3,2,3 anode condition.

One possibility would be that the medium is saturated in the symmetric mode of three anodes (hence the leveling of power out), but the induced asymmetric mode destroys the uniformity of the glow discharge and creates a gradient between the separate glow discharges.

* The general behavior of the 3,2,3 modification mode of 5% Xe at 4 torr is interesting. In contrast to the 5 torr mixture which evolved naturally into an asymmetric mode above 12 mamps, the 4 torr mixture tended to prefer the symmetric mode and would fluctuate between the 3,2,3 mode (higher power) and the symmetric mode (lower power) after the 3,2,3 modification was made.
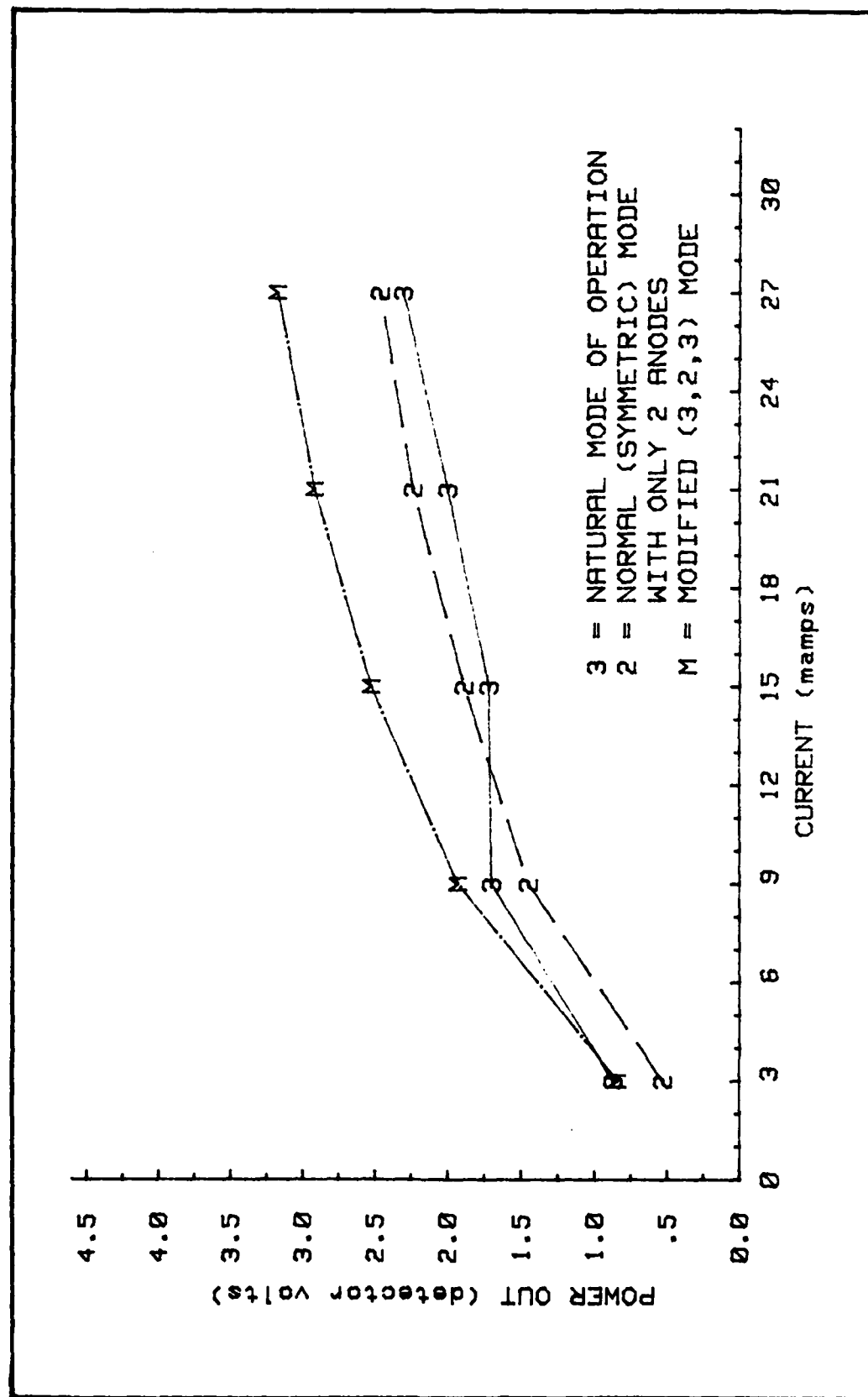
29

Figure 11. Power Curves for 5% Xe at 4 torr with 3 Anodes in the Natural and Modified Modes of Operation and with 2 Anodes

This gradient results in more power out from the laser.

Another experiment was done using 10% Xe at 4 torr. The first run was made with a symmetric current. In the second run, a resistor in the current regulator for the first anode was replaced. Thus, as anodes two and three were varied from 3 to 24 mamps, anode one was varied only from 1.8 to 7.2 mamps. This difference resulted in a deliberate, marked gradient between the first and second anodes. This mode is referenced in this paper as the non-equal current (NEC) mode of operation because the currents are not equal as opposed to the asymmetric mode which has equal currents. As seen in figure 12 (with arbitrary units), the NEC mode continues its increasing power profile after the symmetric mode has leveled.

Due to the time constraints and the preset focus of this experiment, this phenomenon was not investigated further, but is mentioned as an observation for future investigation.

All the remaining data in this thesis was taken with equal currents in the three anodes. All attempts were made to ensure that the symmetric mode or the naturally-evolved asymmetric mode was operating when the power measurements were taken; thus assuring the relationship of the various mixtures and pressures. These modes will also be discussed in conjunction with the power out curves.

Power Comparisons

The power measurements were very consistent and could be duplicated to within a few percent on different days with different fillings of the same mixture and pressure.

The maximum power comparison in figure 13 summarizes the results of this investigation: the optimum mixture and pressure is 10% Xe at
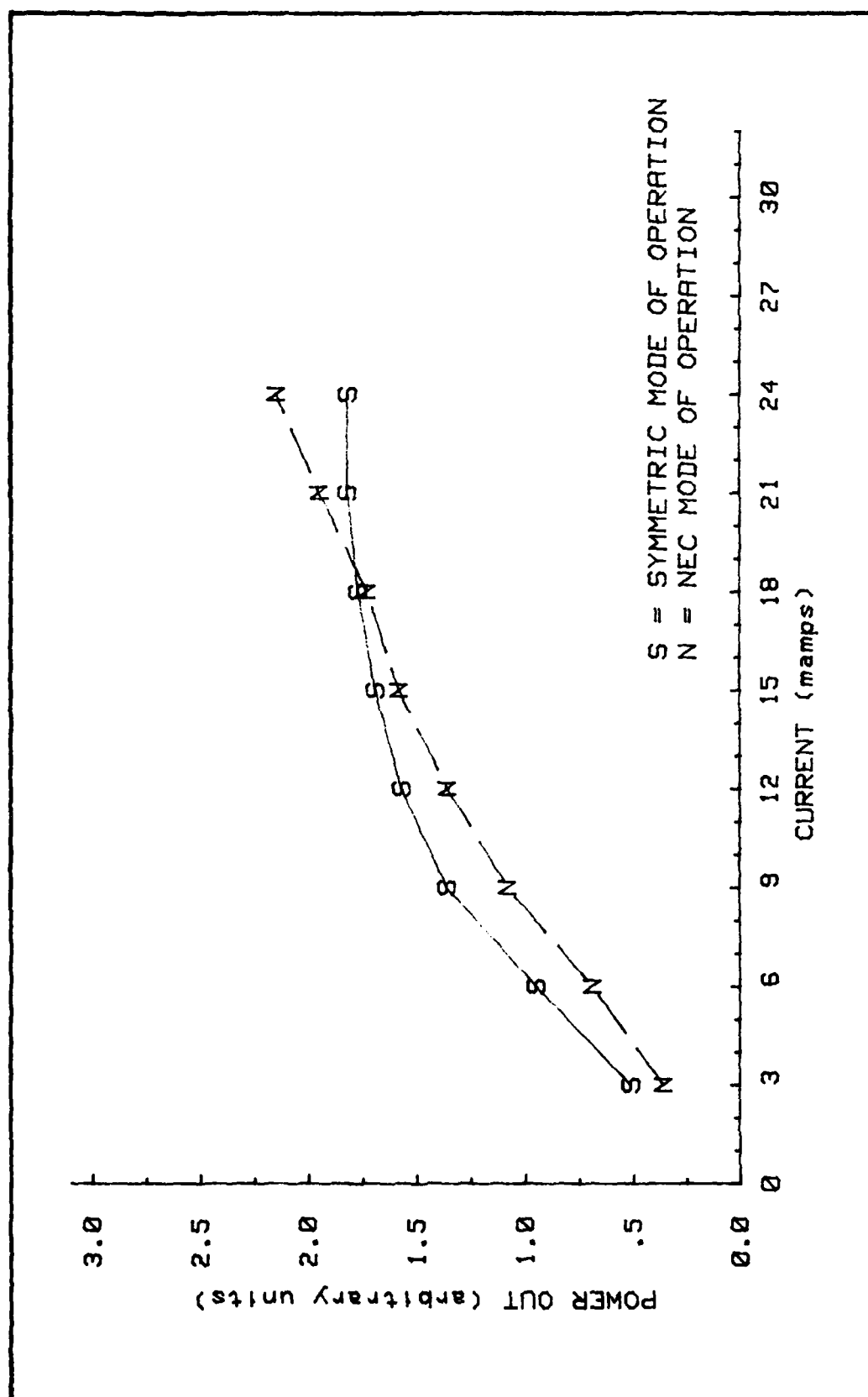
31

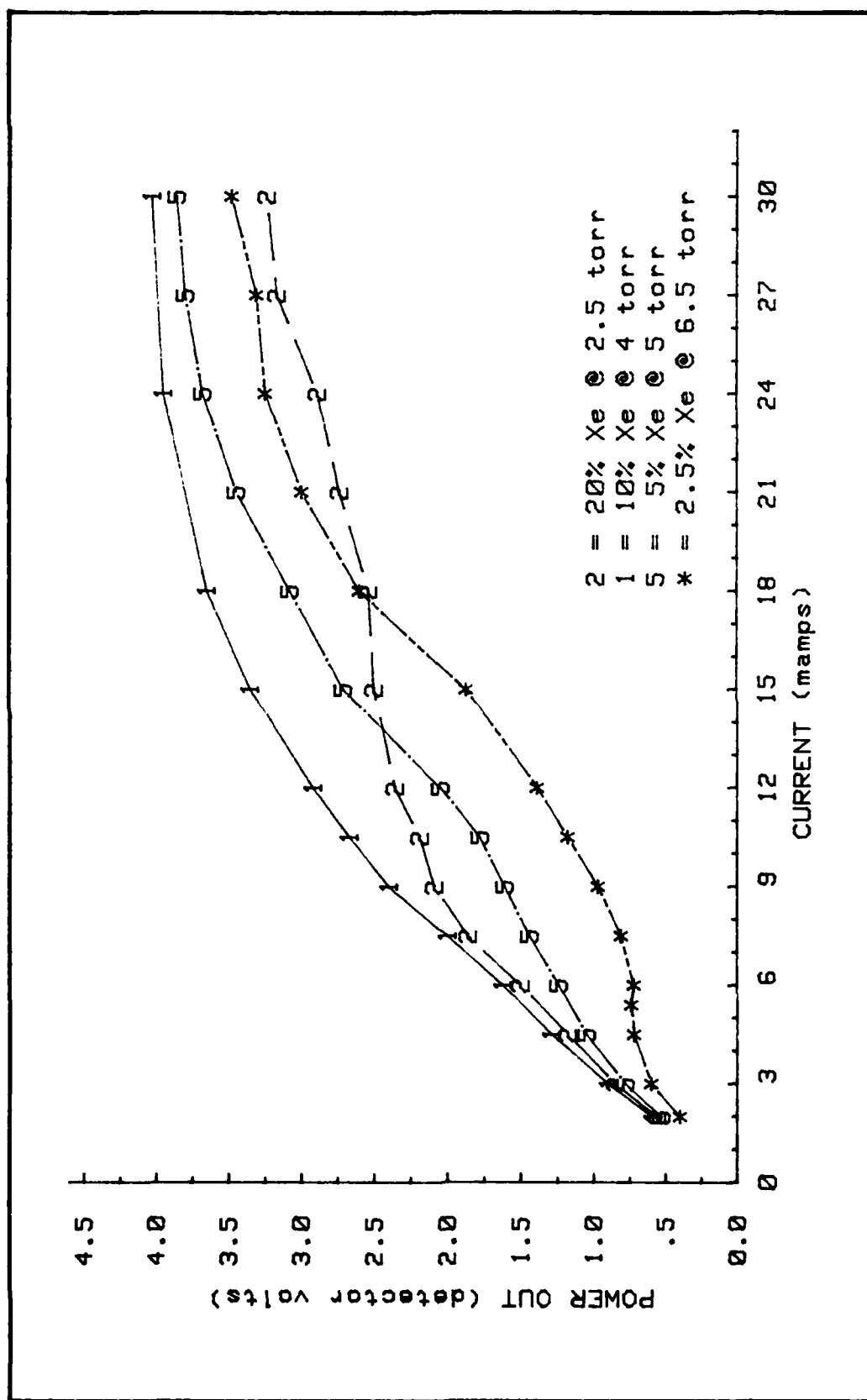Figure 12. Power Curves for 10% Xe at 4 torr in the Symmetric and NEC Modes of Operation

Figure 13. Maximum Power Curves for Mixtures of 20%, 10%, 5%, and 2.5% Xe

4 torr. Measurements at 8% and 11% Xe at 3.5, 4, and 4.5 torr were made to ensure the validity of this value. The resulting maximum powers were all slightly less than the power for 10% Xe at 4 torr.

If the various power curves are compared to one another, many trends become evident. For example, notice the legend in figure 13. As the percentage of Xe increases, the pressure for the maximum power curve decreases. Other trends are obvious when the curves are compared in groups of pressure or mixture.

Pressure Comparisons. At 8 torr (see figure 14), all mixtures have a power dip at the lower end. The current position of these dips is illustrated in table II.

Table II

Current Parameters of 8 Torr Power Dips
With Different Mixtures of Xe

% Xe	CURRENT (BEFORE DIP)	CURRENT (BOTTOM OF DIP)
20	4.1	4.8
10	3.3	4.3
5	3.5	4.5
2.5	4.0	4.6

In the mid-range of 7-12 mamp, the curves show a definite uniformity. The level-off phenomenon of gain saturation affects first 20% Xe at 13 mamps and then 10% Xe at 15 mamps. In table III, the dip data is arranged according to power out in the range immediately after the dip. A trend is more evident: the current position of the dip increases with power out.
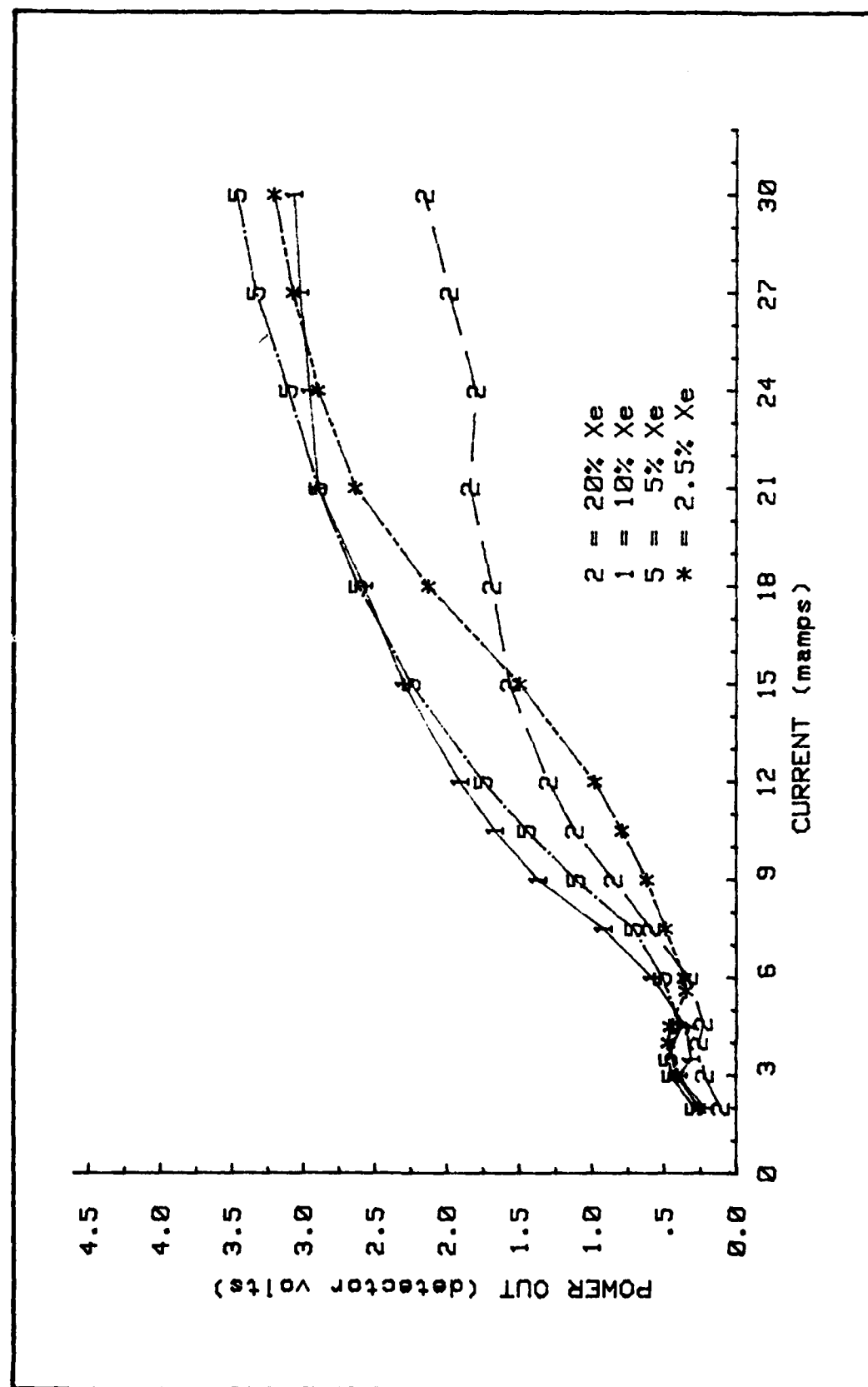
Figure 14. Power Curves for Different Mixtures at 8 torr

Table III

Parameters of 8 Torr Power Dips

% Xe	POWER AT 9 mamps	CURRENT (BEFORE DIP)	CURRENT (BOTTOM OF DIP)
10	1.37	3.3	4.3
5	1.11	3.5	4.5
20	0.87	4.1	4.8
2.5	0.60	4.0	5.6

At 4 torr (see figure 15), power increases with current with each mixture until the leveling phenomenon is more prominent. After 18 mamps, both extremes, 20% and 2.5% Xe mixtures, actually decrease in power out. Meanwhile, the output of the 5% mixture eventually begins another climb and the 10% mixture is just leveling.

At 2 torr (see figure 16), the situation is reversed. The extremes, 20% and 2.5% Xe mixtures, are fairly uniform, but first the 10% Xe mixture and then the 5% Xe mixture decline. At 2 torr, then, the leveling phenomenon appears at a lower current and the evolution of the asymmetric mode does not appear (at least not before the 30 mamp limit of this experiment).

Mixture Comparisons. At 20% Xe (see figure 17), the lower pressures are more efficient. The turning point is 2.5 torr with the maximum power decreasing on either side. It should be mentioned, though, that the 2 torr power out was slightly higher until 4.5 mamps.

At 10% Xe (see figure 18), 2 torr actually declines after approximately 12 mamps. After the power dip of the mode transition of the 8 torr power curve, it parallels the 4 torr curve which is still in the symmetric mode.

At 5% Xe (see figure 19), the 4 torr curve has succumbed to the
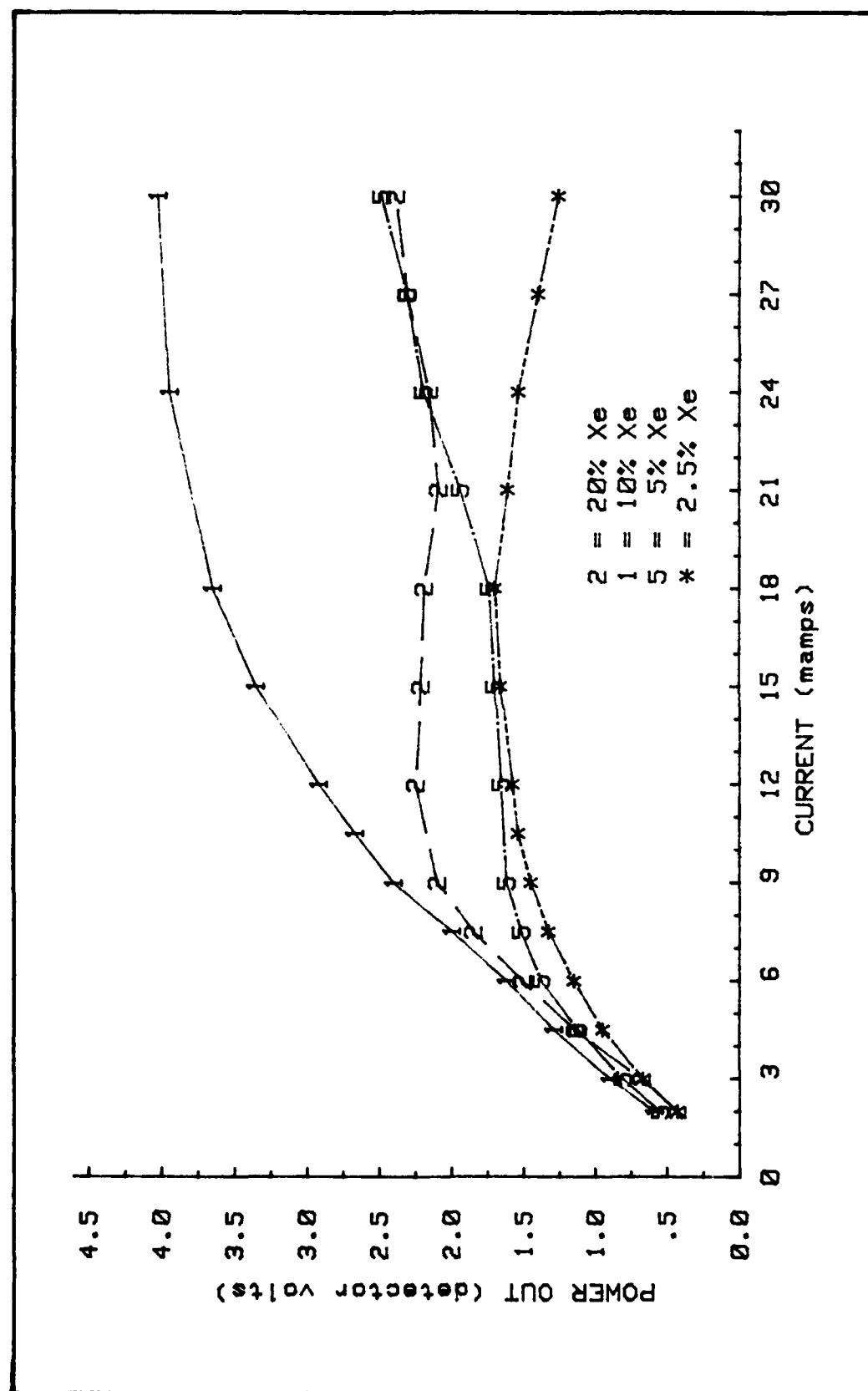
Figure 15. Power Curves for Different Mixtures at 4 torr

37
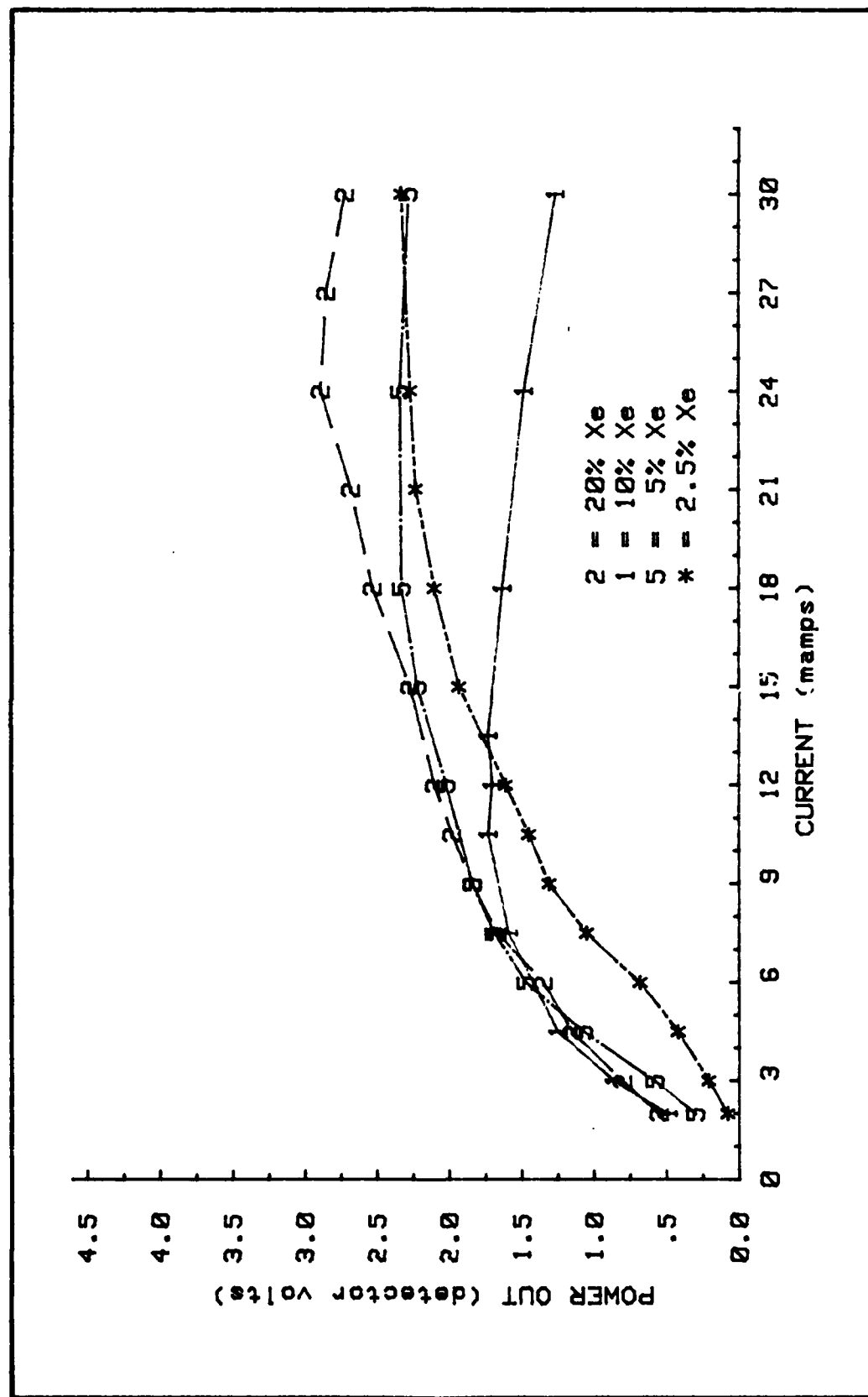
Figure 16. Power Curves for Different Mixtures at 2 torr
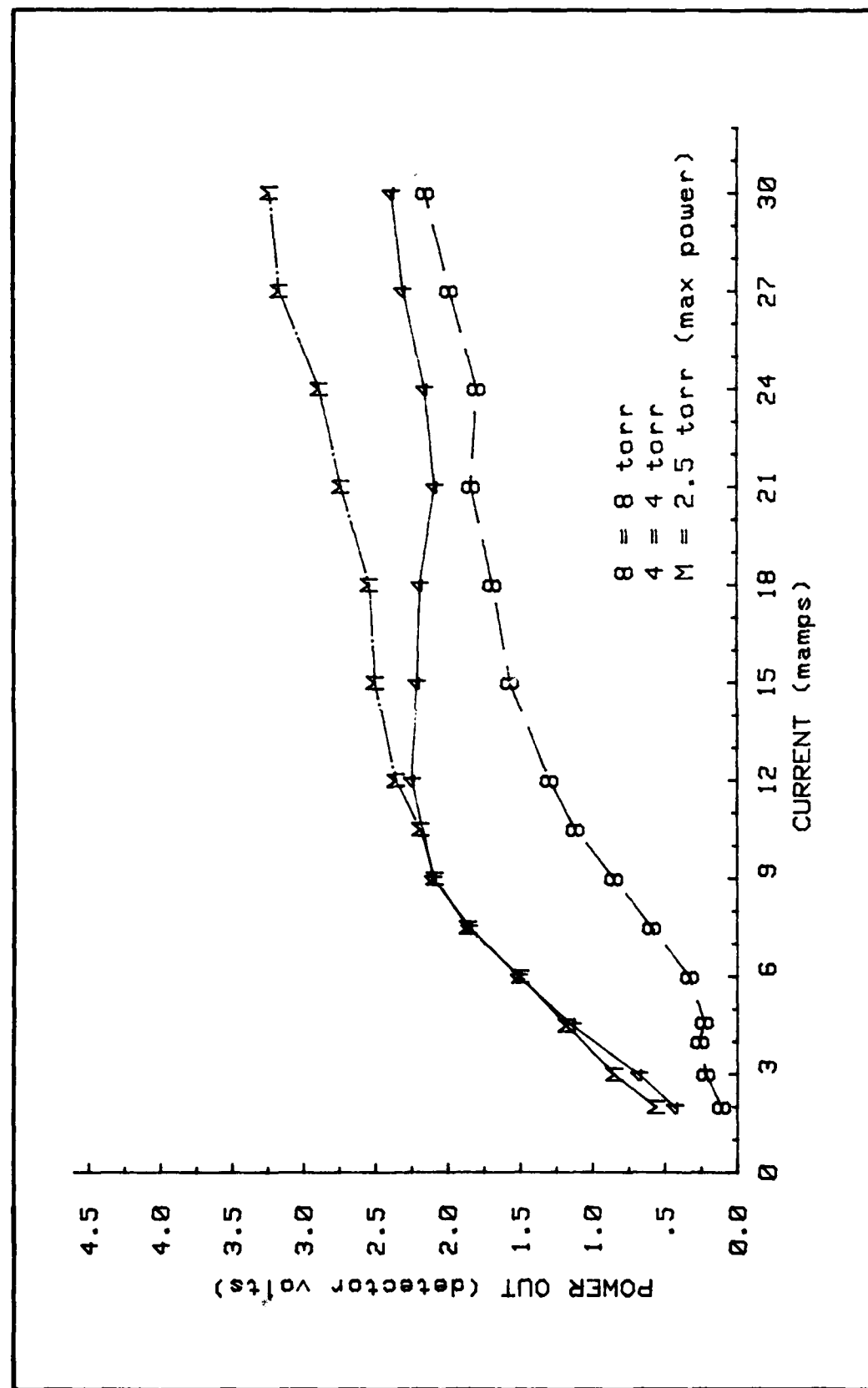
Figure 17. Power Curves for 20% Xe at Different Pressures

8 = 8 torr
4 = 4 torr
M = 2.5 torr (max power)

CURRENT (mamps)

POWER OUT (detector volts)
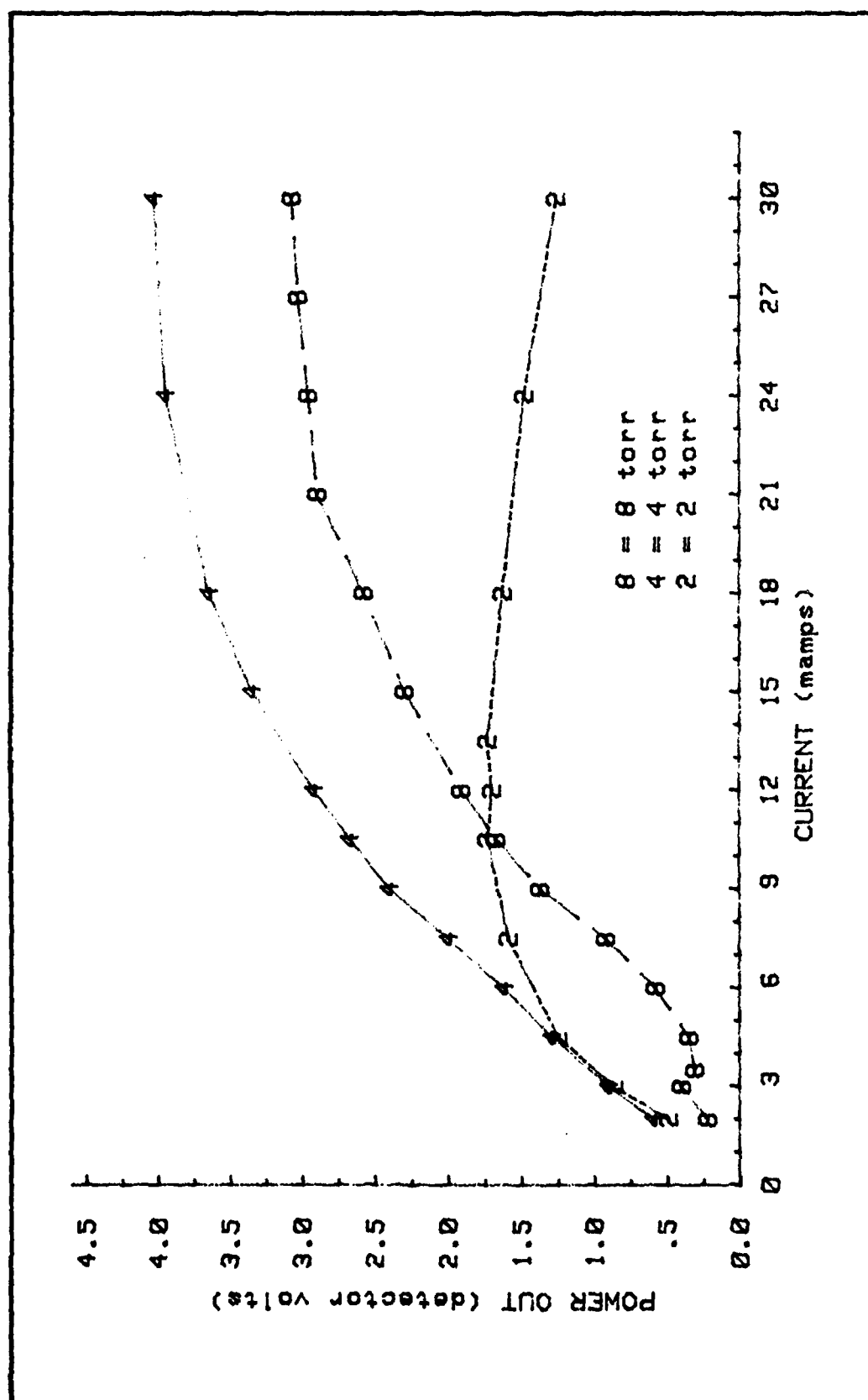
Figure 18. Power Curves for 10% Xe at Different Pressures

8 = 8 torr
4 = 4 torr
2 = 2 torr

CURRENT (mamps)

POWER OUT (detector volts)

40

Figure 19. Power Curves for 5% Xe at Different Pressures

leveling phenomenon and is slow to evolve into the asymmetric mode. However, at 5 torr, the transition to asymmetric is so rapid that the leveling is unnoticeable. (See figure 10.) The 8 torr curve parallels the 5 torr, while the 2 torr pressure remains in the symmetric mode and actually declines rather than transition (before 30 mamps).

At 2.5% Xe (see figure 20), the 6.5 torr of pressure is the survivor and parallels the 8 torr curve, including a slight mode transition dip. The 2 torr power curve is leveling in the symmetric mode and the 4 torr curve fails to transition and merely declines.

Coupler Comparisons. Figure 21 emphasizes the effect of the different output couplers on the optimum mixture and pressure of 10% Xe at 4 torr. Since coupler #1 (R = 89.6%) was the first coupler used, it is used for comparisons. With coupler #2 (R = 79.0%) the power at lower currents was boosted significantly (42% at 3 mamps) while the power at higher currents was less enhanced (4% at 27 mamps). On the other hand, the highly reflective coupler #3 (R = 95.6%) resulted in the same power output at 3 mamps as coupler #1, but the power had a lower rate of increase as current increased. At 27 mamps, output for coupler #3 was only 68% of the output for coupler #1.

Efficiency Comparisons. If one defines the efficiency as the ratio of power out to power in, then (assuming the calculated value 1 dv = 0.254 mw), the efficiency for three anodes is:

Eff = (.254)(detector volts)/[3(anode voltage)(anode current)].

The efficiencies of the maximum power curves (figure 13) are plotted in figure 22. Because the 5% mixture at 5 torr requires less voltage, it is slightly more efficient than the optimum 10% Xe at 4

42
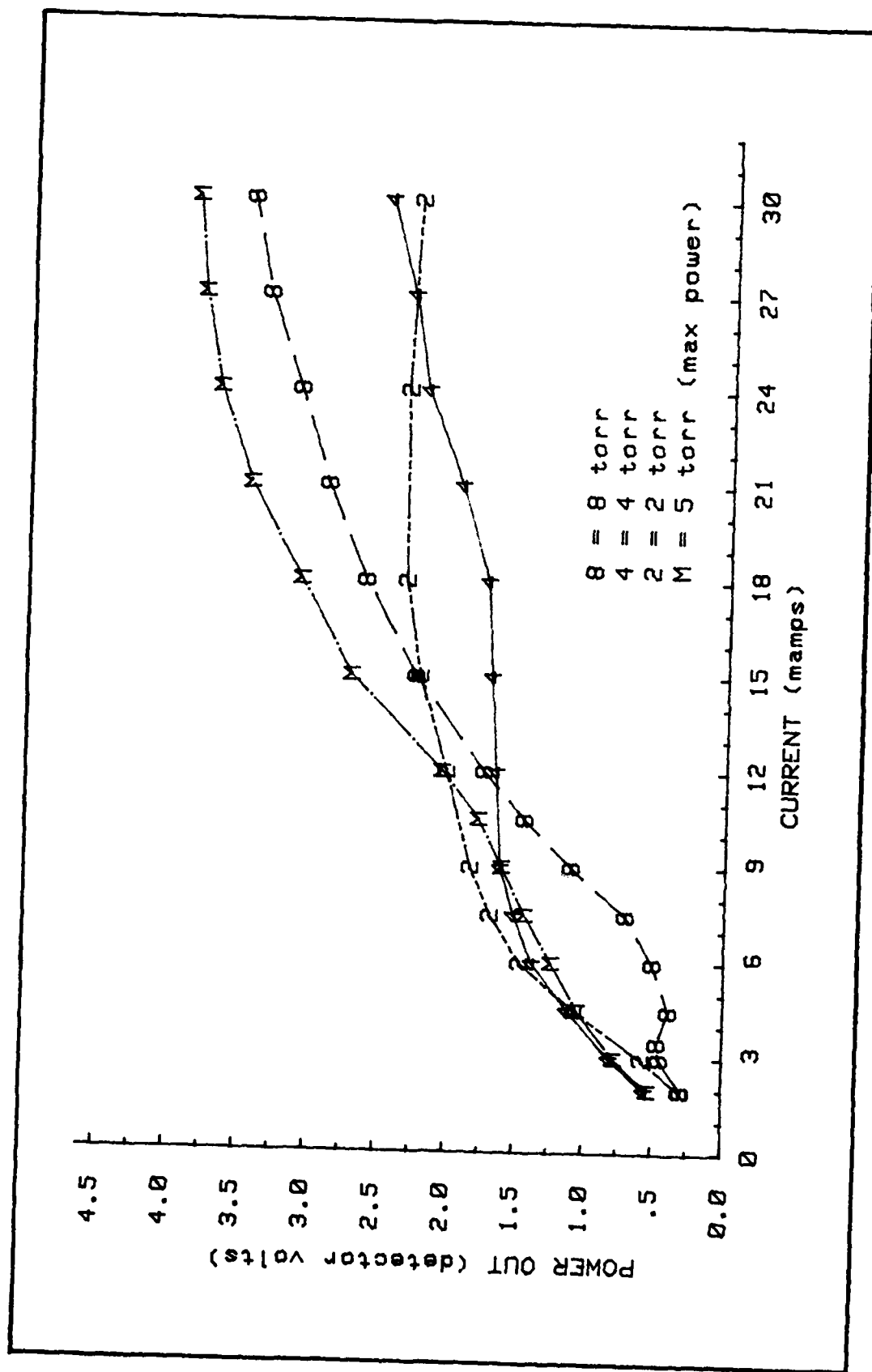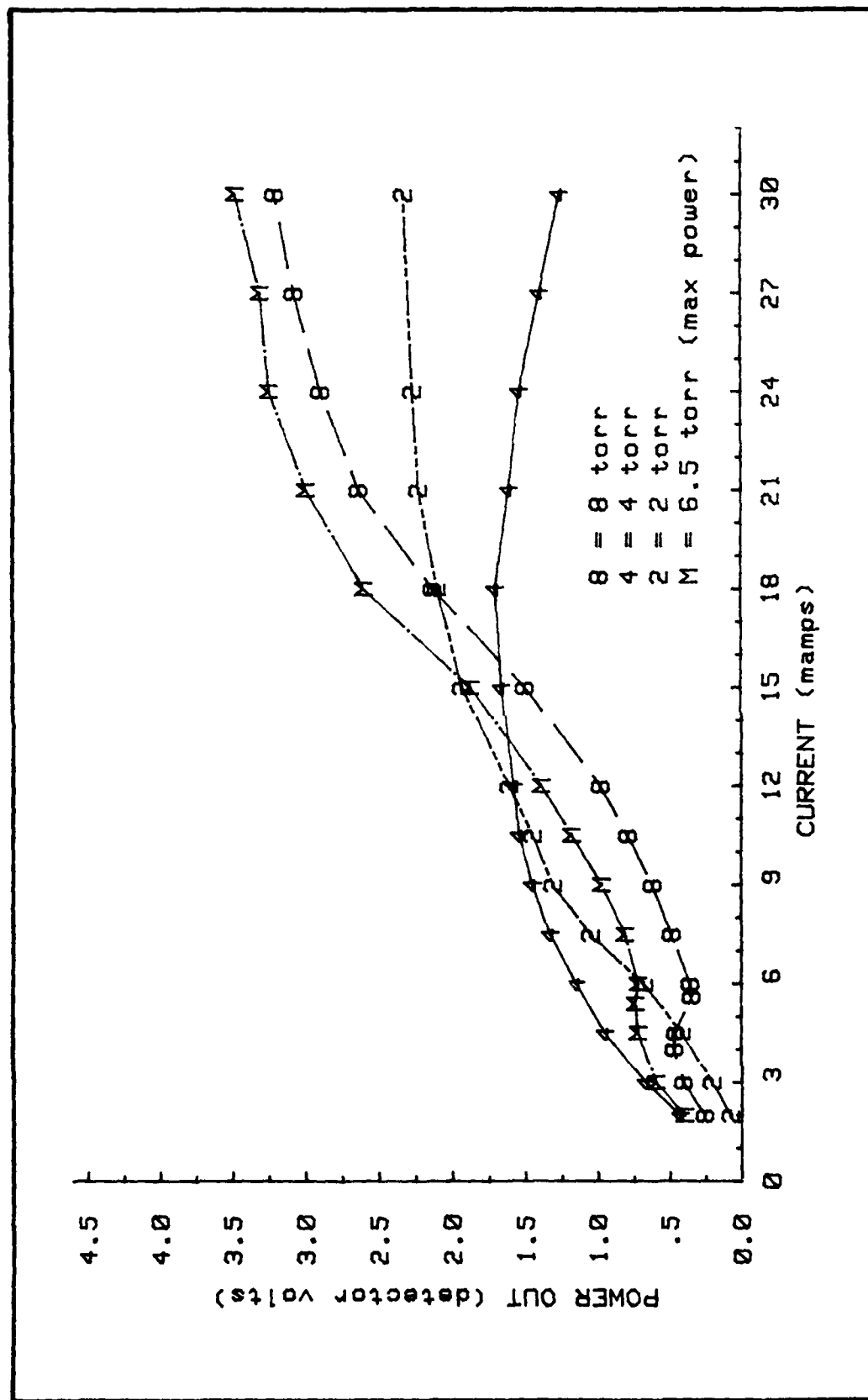
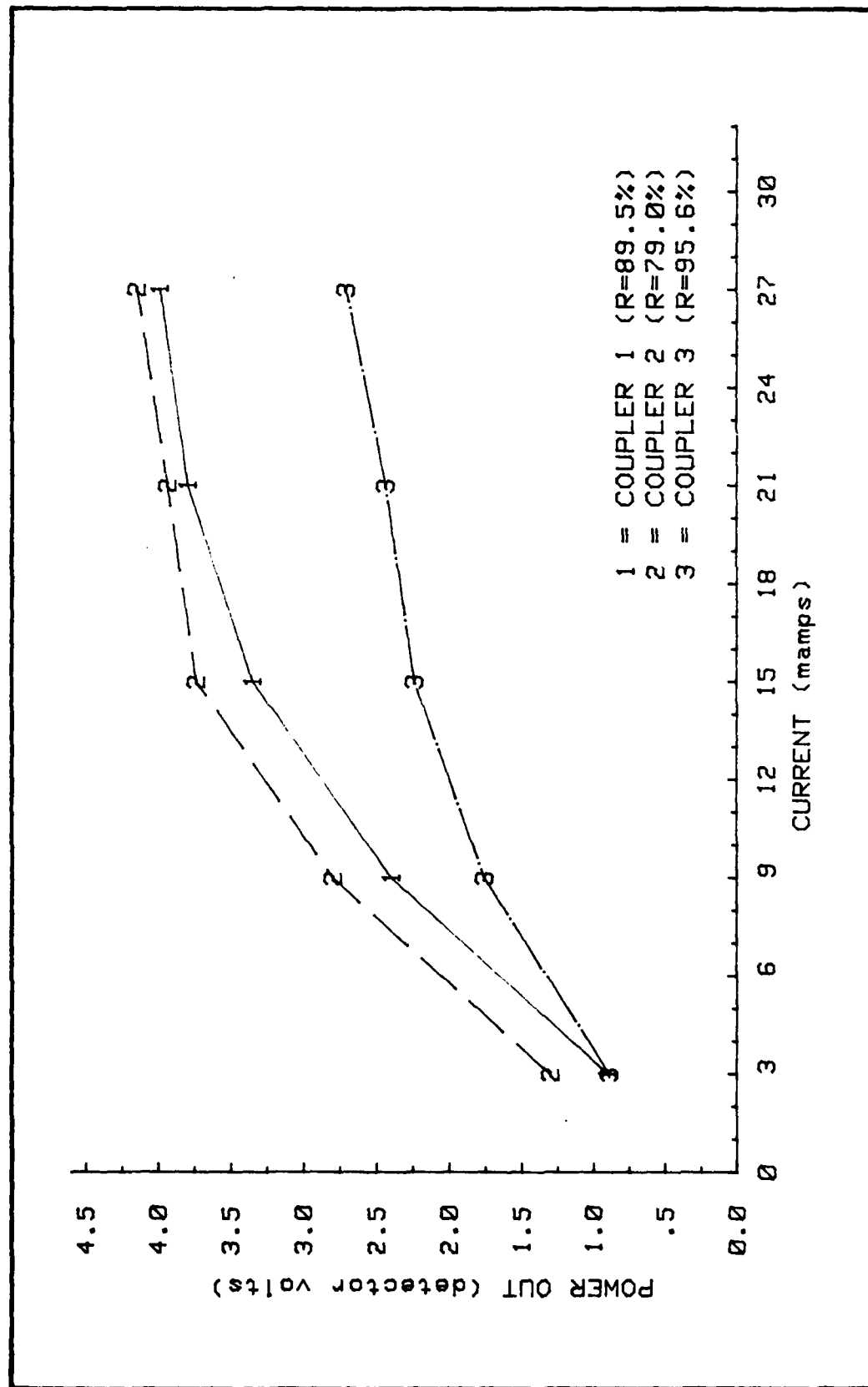Figure 20. Power Curves for 2.5% Xe at Different Pressures

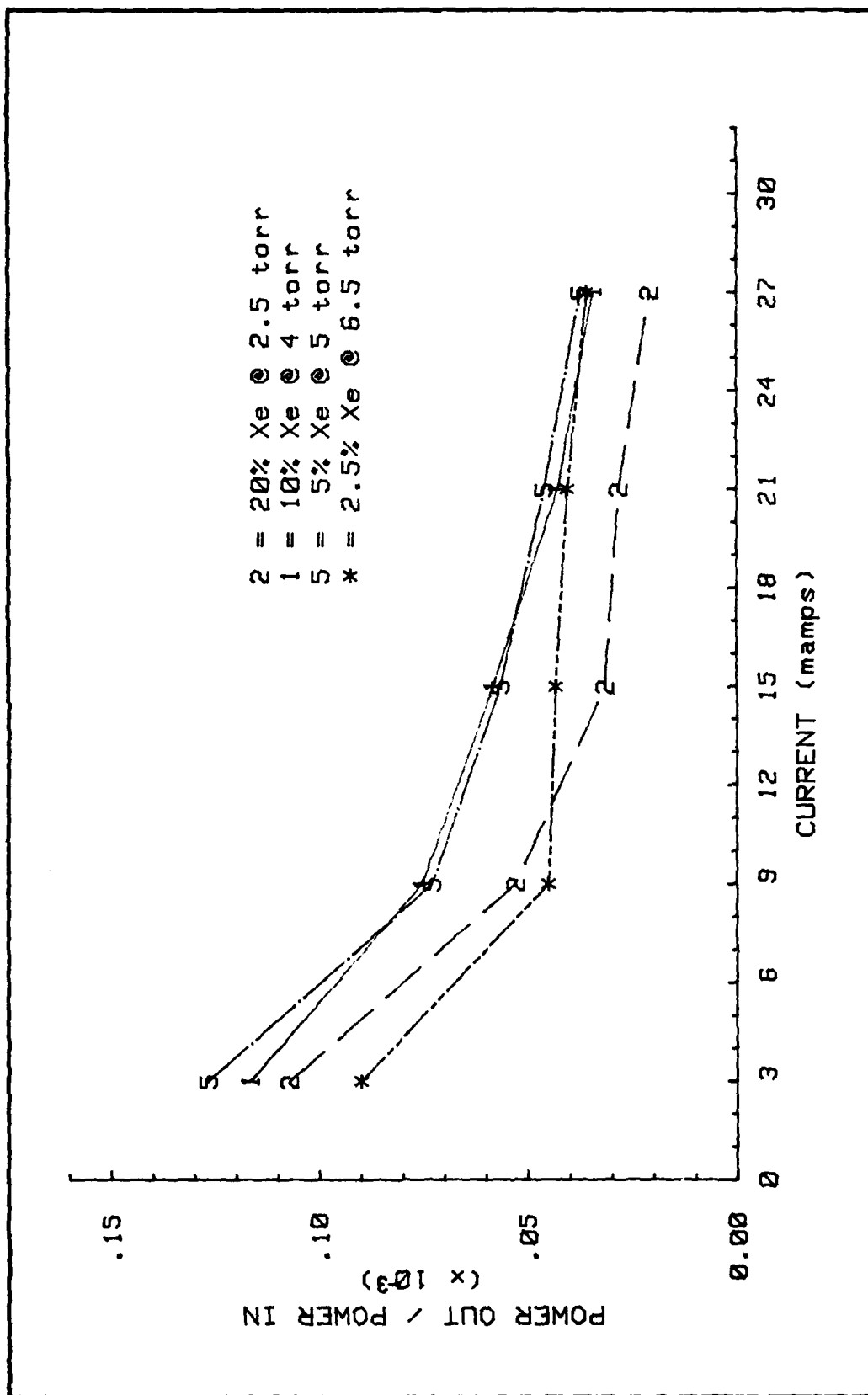Figure 21. Comparison of Power Curves for 10% Xe at 4 torr With Three Different Output Couplers

44

Figure 22. Efficiency for Maximum Power Curves (Assuming 1dv=0.254mw)

45

torr. It is interesting to note that the 2.5%, 5%, and 10% Xe mixtures all converge to a common value.

Figure 23 illustrates the relative efficiencies of the coupler comparison in figure 21. The relationship in figure 23 is so pronounced because the efficiency of the laser is directly proportional to the power out while the power in is the same with each coupler. With coupler #2, the efficiency at 3 mamps is much greater than with coupler #1 because the difference in power out is so great. At 27 mamps, the efficiencies are about the same. On the other hand, the efficiency of coupler #3 is the same as coupler #1 at 3 mamps, but then decreases more rapidly.

Gain and Loss Measurements

Windows of various transmittances at 3.51 µm were inserted into the cavity slightly away from normal. Power out was plotted against $-\ln(Ta^2)$. Transmissivities at 3.51 µm were obtained by averaging at least four values of I/Io outside the cavity. For severe losses, four microscope slides were used. Their transmissivities were 0.543, 0.499, 0.495, and 0.484. Three thin quartz windows with transmissivities of 0.904, 0.890, and 0.875 and a thicker quartz window of T = 0.817 were used for more moderate attentuation and hence better curve fitting. The resulting data was fit by the method of least squares to equation #26.

All measurements were taken at the optimum mix and pressure: 10% Xe at 4 torr. For comparison, the gain and loss parameters were investigated at both low and high currents with coupler #3 (R = 0.956). For contrast, a high current measurement was also taken with coupler #2 (R = 0.790). For consistency during the lengthy process, the current

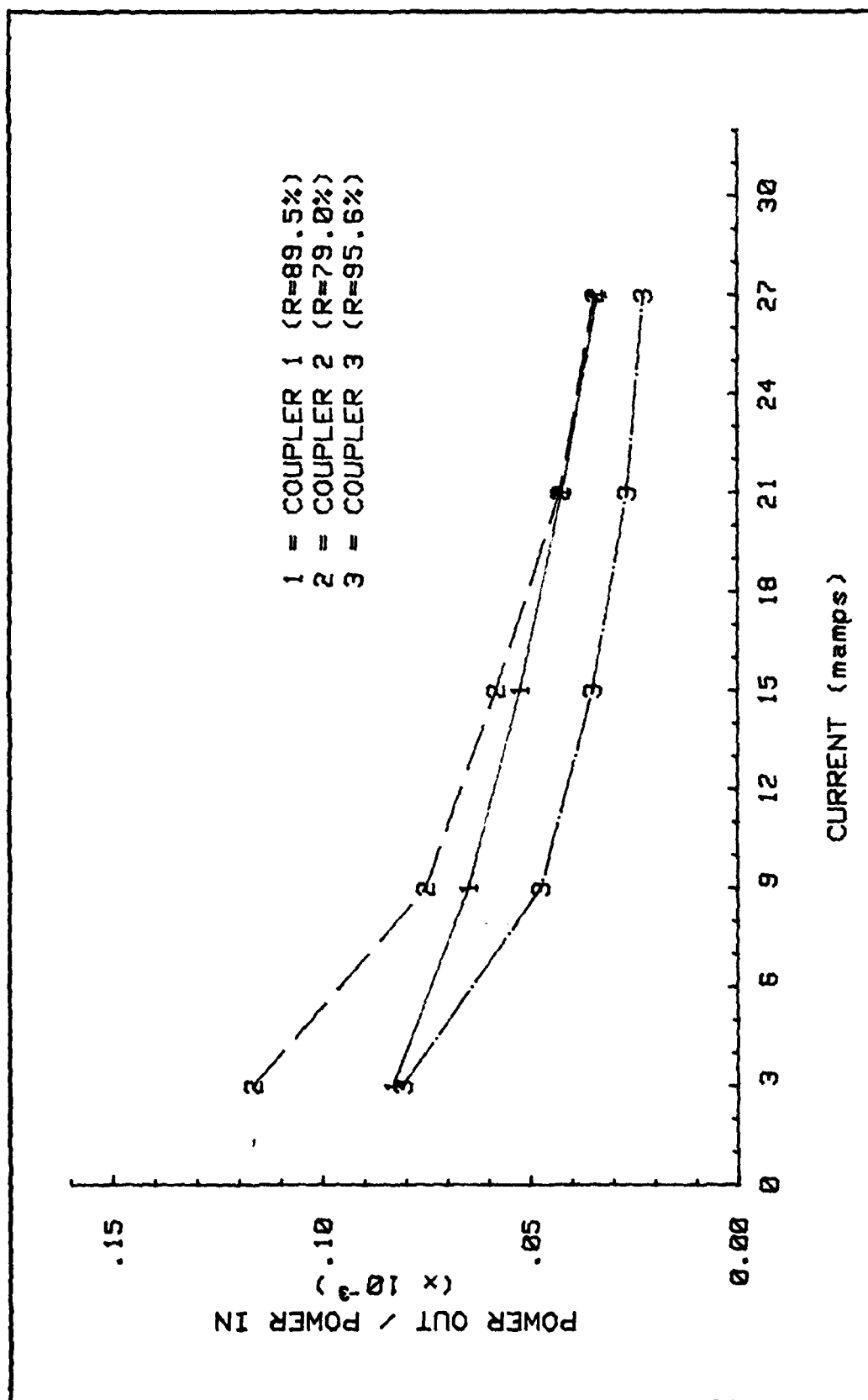Figure 23. Efficiency for Power Curves of 10% Xe at 4 torr With Three Different Output Couplers

47

was varied slightly to maintain the reference power.

Curve Fit Method. The first set of measurements was made with

R = 0.956, current = 7 mamps, and power out = 1.31 dv. The data is

plotted in figure 24. The least squares fit of equation #26 yields:

$a = 9.972 \times 10^{-2}$; $g = 1.988$; and $C = 6.912 \times 10^{-2}$.

Hence, (from equation #28) $Li = 1 - [(\exp(-a)/(1-T)] = 5.33\%$ and

(from equation #25) $Ropt = \exp[Li - \sqrt{(g \times Li)}] = 76.17\%$.

The second set of measurements was made with R = 0.956, current =

25 mamps, and power out = 2.5 dv. The data is plotted in figure 25.

Least squares fit: $a = 9.546 \times 10^{-2}$; $g = 1.724$; and $C = 0.1464$. Hence,

$Li = 4.92\%$ and $Ropt = 78.50\%$. Table IV is a comparison of theoretical

power out using equation 30 with the interpolated (straight line) data.

TABLE IV

Comparison of Theoretical and Interpolated Power
Using First and Second Measurement Data

OUTPUT COUPLER #	R [%]	THEORETICAL POWER [dv]	INTERPOLATED POWER [dv]	% DIFF.
1	89.5	1.87	1.79	4.73
2	79.0	2.12	2.30	8.69
3	95.6	1.31	1.31	0.09
1	89.5	3.49	3.74	7.74
2	79.0	3.85	4.08	5.90
3	95.6	2.50	2.50	0.10

However, the third set of data proved to be perplexing. The

plotted data for R = 0.790, current = 25 mamps, and power out = 3.9 dv

is plotted in figure 26. The least squares fit (solid line) yielded:

$a = 2.523 \times 10^{-1}$; $g = 1.850$; and $C = 6.136 \times 10^{-1}$. However, the resultant

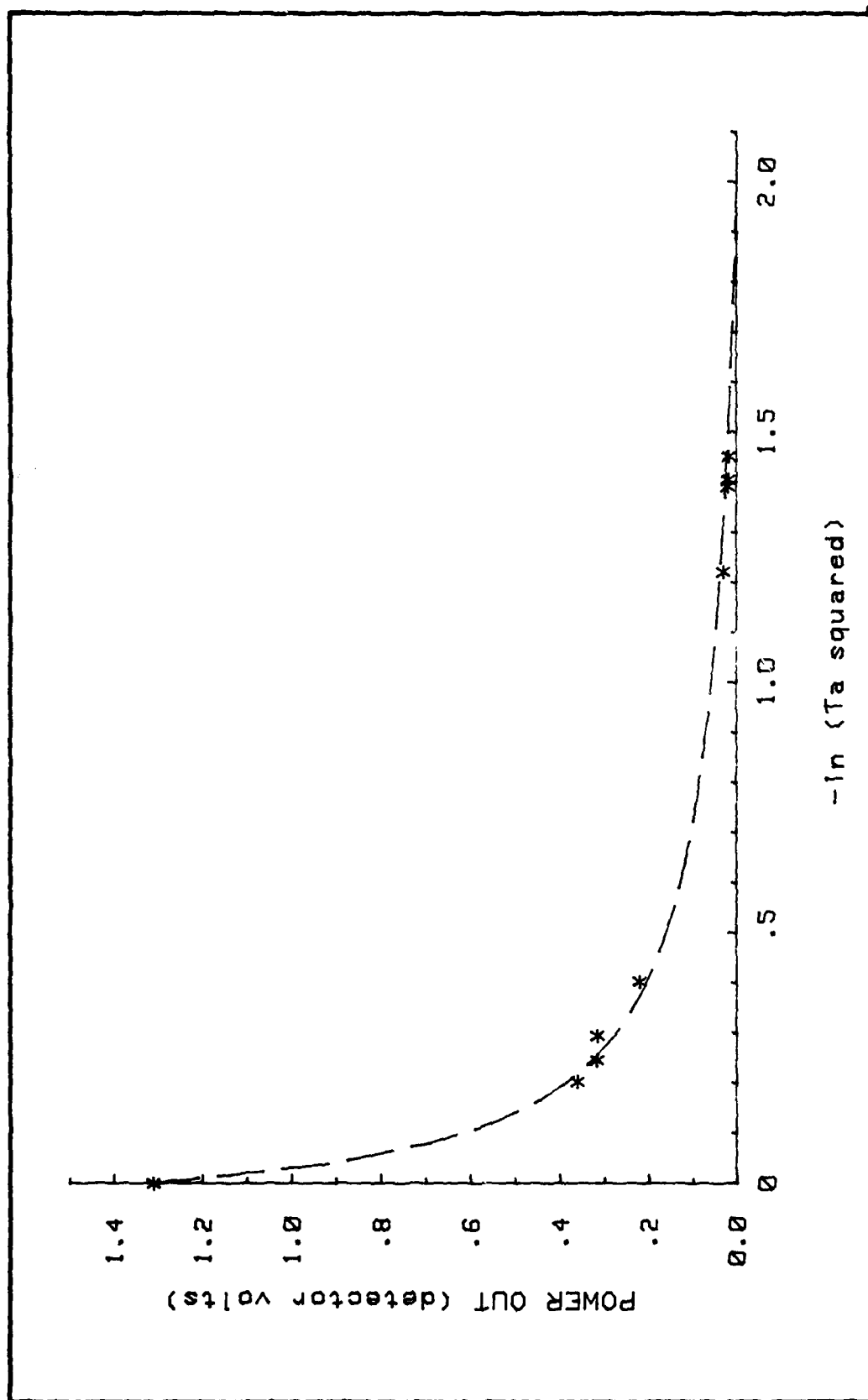$Li = 1.64\%$ is implausible for this laser and greatly in variance with

Figure 24. Power Measurements for Low Current (7 mamps) With High Reflectivity (R=95.6%) Output Coupler
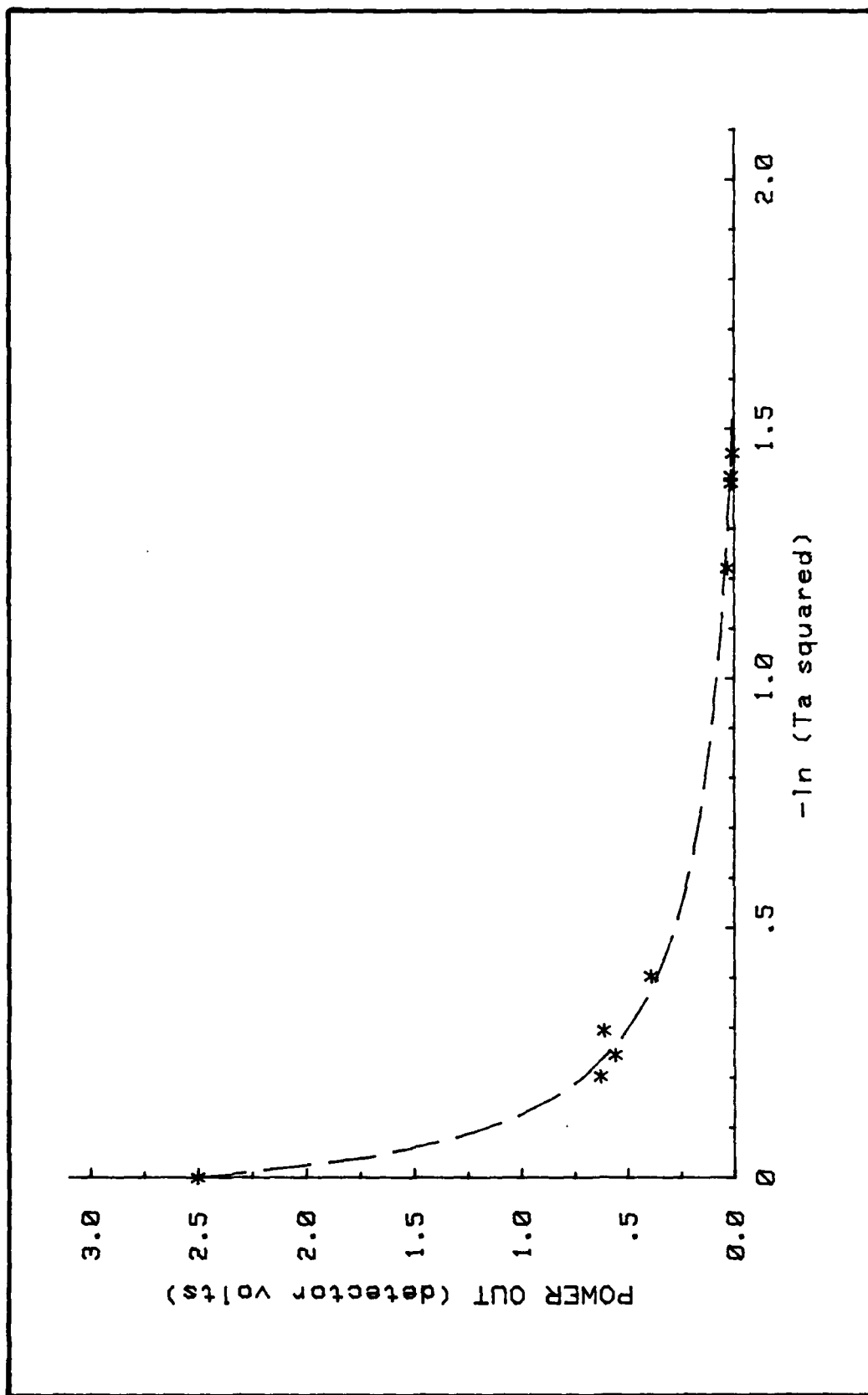
Figure 25. Power Measurements for High Current (25 mamps) With High Reflectivity (R=95.6%) Output Coupler
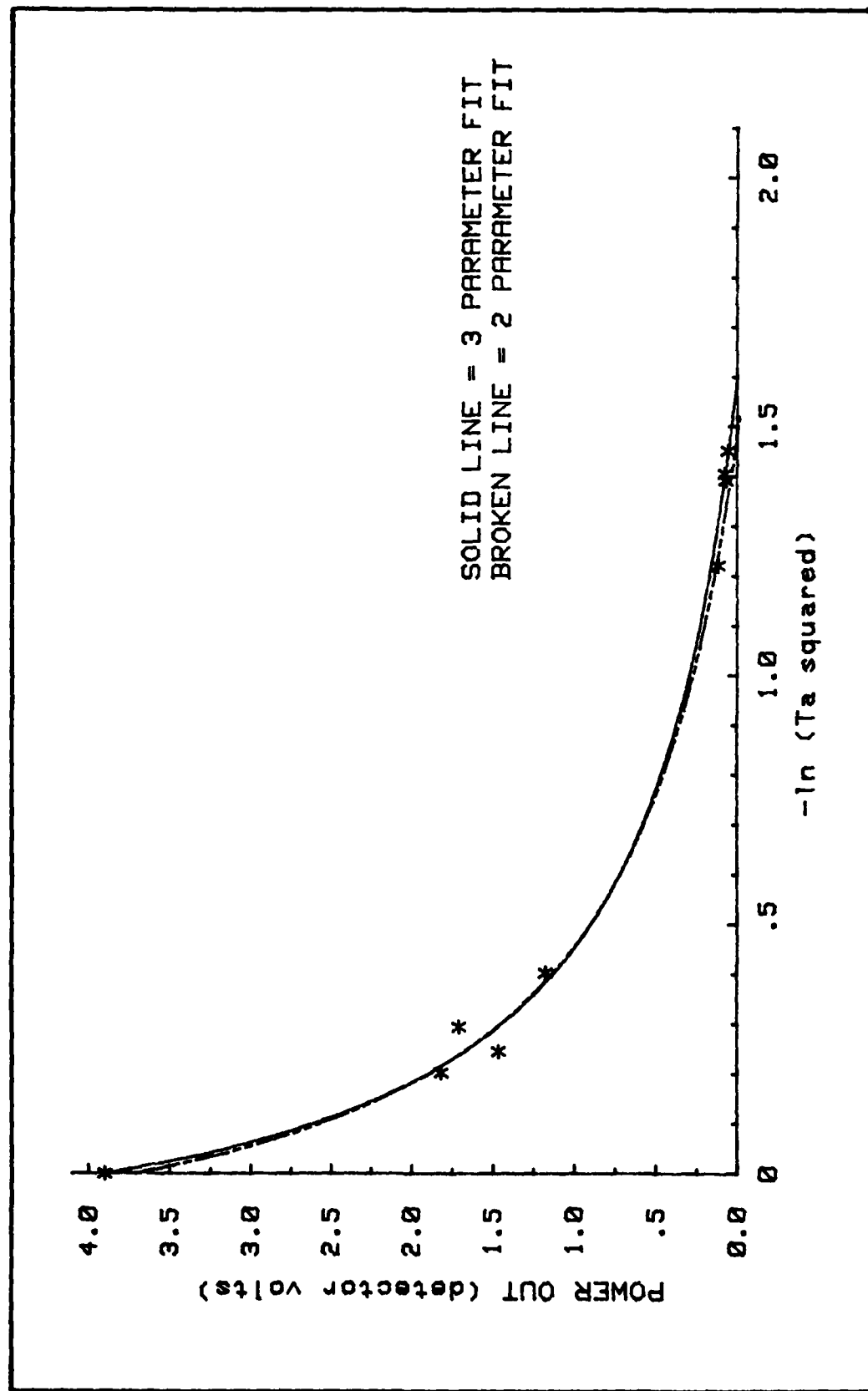
Figure 26. Power Measurements for High Current (25 mamps) With
Low Reflectivity (R=79.0%) Output Coupler

51

the earlier calculations. Also, the calculated Ropt = 85.40% is contrary to the experimental results. Note also the large discrepancy in the theoretical power in table V.

TABLE V

Comparison of Theoretical and Interpolated Power
Using Third Measurement Data

OUTPUT COUPLER #	R [%]	THEORETICAL POWER [dv]	INTERPOLATED POWER [dv]	% DIFF.
1	89.5	3.90	3.74	4.32
2	79.0	3.88	3.90	0.51
3	95.6	3.40	2.50	36.14

If, however, the Li is fixed at 5.125% (the average of the first two), the two-parameter least squares fit (the dotted line in figure 26) is still very close to the first curve, but g = 1.788 and C = 7.320×10^{-1}. Compare the values in table VI.

TABLE VI

Comparison of Theoretical and Interpolated Power
Using Two-Parameter Fit Data of Third Measurement

OUTPUT COUPLER #	R [%]	THEORETICAL POWER [dv]	INTERPOLATED POWER [dv]	% DIFF.
1	89.5	3.42	3.74	9.30
2	79.0	3.81	3.90	2.44
3	95.6	2.42	2.50	3.31

In fact, it is reasonable to apply the average loss to the first two cases as well. When a two-parameter forced fit is applied with Li = 5.125%, the plotted curves are indiscernible from the three-parameter fits. Table VII compares the 1.31 dv data, (g = 2.058 and

52

C = 6.542×10^{-2}) a the 2.5 dv data (g = 1.681 and C = 1.536×10^{-1}).

TABLE VII

Comparison of Theoretical and Interpolated Power Using
The Average Li – 5.125% for Low and High Current Data

Ropt	OUTPUT COUPLER	THEORETICAL POWER [dv]	INTERPOLATED POWER [dv]	% DIFF.
76.07%	1	1.86	1.79	4.09
	2	2.10	2.30	9.64
	3	1.31	1.31	0.02
78.49%	1	3.51	3.74	6.44
	2	3.89	4.08	4.98
	3	2.49	2.50	0.33

Thus, for Li = 5.125%, the average difference between theoretical and interpolated power is 4.51% for g = 2.06 at 7 mamps and average g = 1.73 at 25 mamps.

Taking the process a step further and performing forced fits for several values, 4.92% < Li < 5.33%, the least variation of the average difference between theoretical and interpolated power is 3.72% when Li = 4.92% for all coupler data. It is therefore most reasonable to accept the following:

Li = 4.92%; g = 2.14 at 7 mamps; and g = 1.75 at 25 mamps.

Alternate Method. The alternate method of gain measurement takes a linear regression of the points on the tail of the curve. Since four points were measured in this area, a fair approximation is possible. Table VIII compares this value with the calculated quantity x = g-a from the first method.

TABLE VIII

Comparison of the Curve Fit and Alternate Methods
of Parameter Determination

CURRENT	R [%]	X-INTERCEPT	CALCULATED	% DIFF.
7 mamps	95.6	1.750	1.960	12.02
25 mamps	95.6	1.541	1.583	2.73
25 mamps	79.0	1.693	1.500	12.87

Twelve percent difference would provide a good start for a non-linear regression. Note however, that the calculated x-intercept for the three-parameter fit of the R = 79.0% data would be 1.598, which is only 5.94% different. This value is deceptively close; deceptive because Li = 1.64% is implausible in this laser. Thus, the limitation of the alternate method is again brought to light. It merely reveals the quantity $x = g-a$. Unless a minimum variation of $Pj = C[g/(a+x) -1]$ is iterrated between the three couplers, one could only say that $g-a = 1.69$.

Supplementary Observations

In this experiment, many phenomena were observed which were not directly related to the other four divisions of this analysis section. They are, however, items of interest which should not be left unmentioned. These observations fall under the categories of temperature dependence, contaminants, beam uniformity, and gas breakdown.

Temperature Dependence. The power appeared to have a definite dependence on the temperature measured at the external surface of the hollow cathode. The power would regularly increase during the temperature ranges of 38-42°C, 48-52°C, and 57-60°C. The laser power would reach a higher plateau at each of these ranges.

54

Contamination. The He-Xe is extremely sensitive to any contamination within the hollow cathode. With the least contamination (via system leaks) the power output would be generally lower, would rise more slowly, and would actually decline after about 12 mamps, much like a symmetric mode which will not evolve into an asymmetric mode. For example, a small leak developed at the aft brewster window in this laser. It was only large enough for the diffusion pump to be unable to pump below 1.7×10^{-7} torr and yet the laser displayed these typical characteristics of contamination. After fixing the leak, anode voltage decreased and power increased yielding better efficiency. Until completely outgassing the contaminants, the power decreases with the laser valve closed. Opening the laser valve creates a reservoir effect and decreases the partial pressure of the contaminant in the glow discharge.

Beam Uniformity. As mentioned earlier, the laser beam appeared to have "hot spots" which could be painstakingly focused onto the detector. If one of the anodes was disconnected, the power of such a hot spot would rapidly increase as much as 54%. On the other hand, these hot spots would decrease in intensity as the temperature of the tube increased.

Gas Breakdown. At lower pressures the gas discharge was more difficult to initiate. This was more pronounced at lower mixtures of Xe. For example, 10% Xe at 1 torr would require high current and voltage settings for gas breakdown, while at 2.5% Xe, 2 torr would be the lowest pressure for gas breakdown. This also led to a hysteresis-type effect in the power curve. As seen in figure 27, when current was decreased, the power remained up until one anode failed to break-
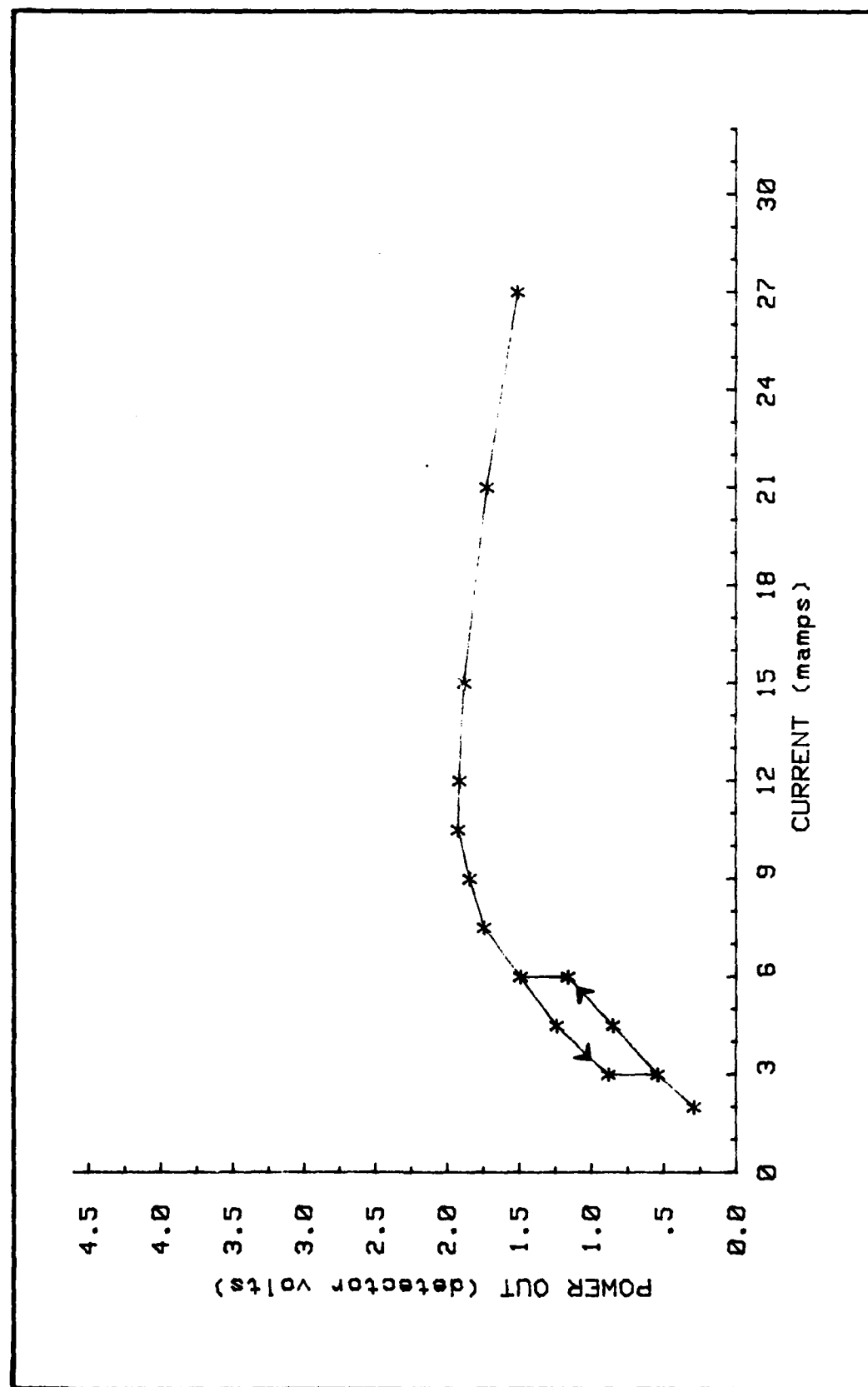
55

Figure 27. Hysteresis-Type Effect in the Power Curve of 10% Xe at 2 torr

down the gas. As the current was then increased, the power would stay down until the anode resumed its usefulness.

Discharge Irregularities. With 20% at 4.5 torr, an irregularity was noted in the physical characteristics of the discharge within the tube. At 3 mamps (per anode), the glow discharge appeared normal within the hollow cathode tube. As the current was increased to 21 mamps, the bright glow discharge advanced to fill the entire hollow cathode tube from brewster window to brewster window. At 24 mamps, a small jet of bright discharge was seen at the junction of the side arm and the hollow cathode tube. Figure 28 illustrates the flame-shaped cone extended into the axial portion of the glow discharge. As the bellows valve was moved from the open to the closed position, every-thing was stable until 1½ turns before sealing. At this point, the glow discharge dimmed significantly and "jumped" back from the brewster windows. As the valve was sealed, the glow discharge jumped back to a point halfway to the brewster windows, and the glow intensity increased again. Table IX contains a synopsis of the events.

TABLE IX

Power and Anode Voltage Comparison at Different
Valve Positions with 20% Xe at 4.5 Torr

VALVE POSITION	POWER [dv]	ANODE VOLTAGES		
		#1	#2	#3
Open	2.06	328	359	357
1½ Turns before sealing	2.10	321	359	357
Closed	2.20	332	360	357

AXIAL VIEW:

vacuum system
side arm

—————inside wall of tube

------- negative glow boundary
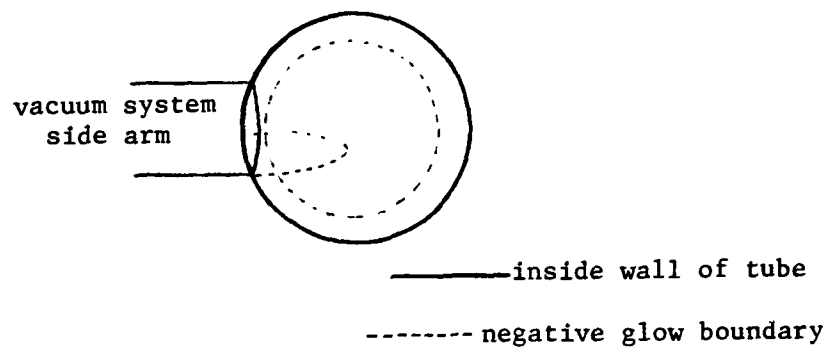
LONGITUDINAL VIEWS:
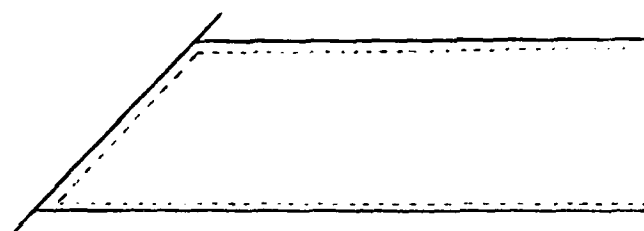
a. with valve open;

b. 1½ turns before sealing;

c. with valve sealed.

Figure 28. Physical Characteristics of HCD at 24 mamps

Because this phenomenon was observed late in the experiment, further investigations of it were not possible. It would appear, though, to be further manifestations of the modes of operation theory developed earlier in this thesis.

V SUMMARY AND CONCLUSIONS

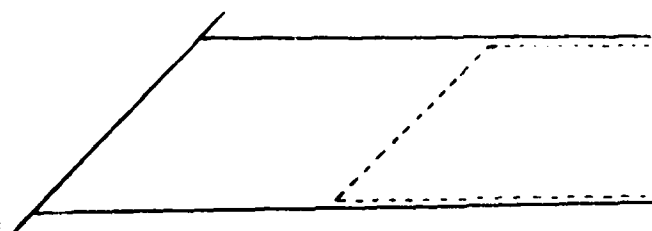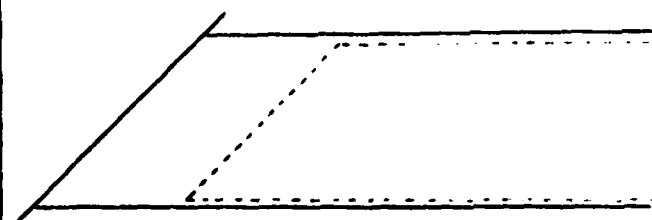The He-Xe hollow cathode discharge laser is an infrared laser which oscillates at 3.507 μm. The small size and minimal power requirements of this laser make it an ideal probe laser. Power and anode voltage measurements were within 3% from day to day and from filling to filling.

The He-Xe HCD laser operates in definite symmetry modes. The symmetric mode of operation is characterized by equivalent voltages driving the anodes at the same current. The asymmetric mode is produced when the plasma extends out of the axial portion of the hollow cathode and is characterized by lower voltage at that anode. The non-equal current (NEC) mode of operation is obtained by operating one or more of the anodes at different currents.

The He-Xe HCD is more powerful in the symmetric mode until saturation is reached. As current is further increased, either power declines or the asymmetric mode evolves. After saturation in the symmetric mode, the asymmetric mode produces more power. After saturation, the NEC mode of operation is also more powerful than the symmetric.

The use of internal mirrors in lieu of brewster windows would reduce the internal losses and could increase the power. However, assuming the brewster windows account for a total of 1% loss, application of equation #30 indicates only a 4% power increase. This minimal gain may be insufficient to outweigh the disadvantages of internal mirrors. One disadvantage is that internal mirror coatings tend to erode in the active medium of a laser. Another disadvantage is that some of the Xe lines now inhibited by the calcium fluoride brewster

60

windows would no longer be inhibited and could degrade the desired laser line.

Figure 29 illustrates the optimum reflectance for an output coupler with the laser operating at 7 mamps or 25 mamps. In the current configuration, the optimum coupler for this laser is 78.3% or 75.9% with the discharge current at 25 mamps or 7 mamps, respectively. Again, though, the "optimum coupler" would not enhance the current output more than 4% over the current coupler #2 (R = 79.0%) and would probably not be worth the cost.

The maximum power out for this He-Xe hollow cathode discharge laser is achieved with 10% Xe at 4 torr of pressure. At 27 mamps, this combination yields 4.15 dv (1.05 mw) with the valve closed or 4.55 dv (1.16 mw) with the valve open.

If efficiency is the main concern, though, 5% Xe at 5 torr is almost as powerful at 27 mamps, but requires less voltage and is therefore most efficient.

Unfortunately, the higher currents cause high temperatures in the system. The hollow cathode can reach 60°C within two minutes. If this maximum power is required, some temperature controls will be necessary. Finned jackets radiating to forced air may be sufficient. If not, water cooling will maintain temperatures.

Stable temperatures between 31°C and 46°C can be maintained between 3 mamps and 9 mamps, respectively. In this range, the most power out is 2.91 dv (0.74 mw) at 9 mamps with 9% Xe at 4.5 torr.
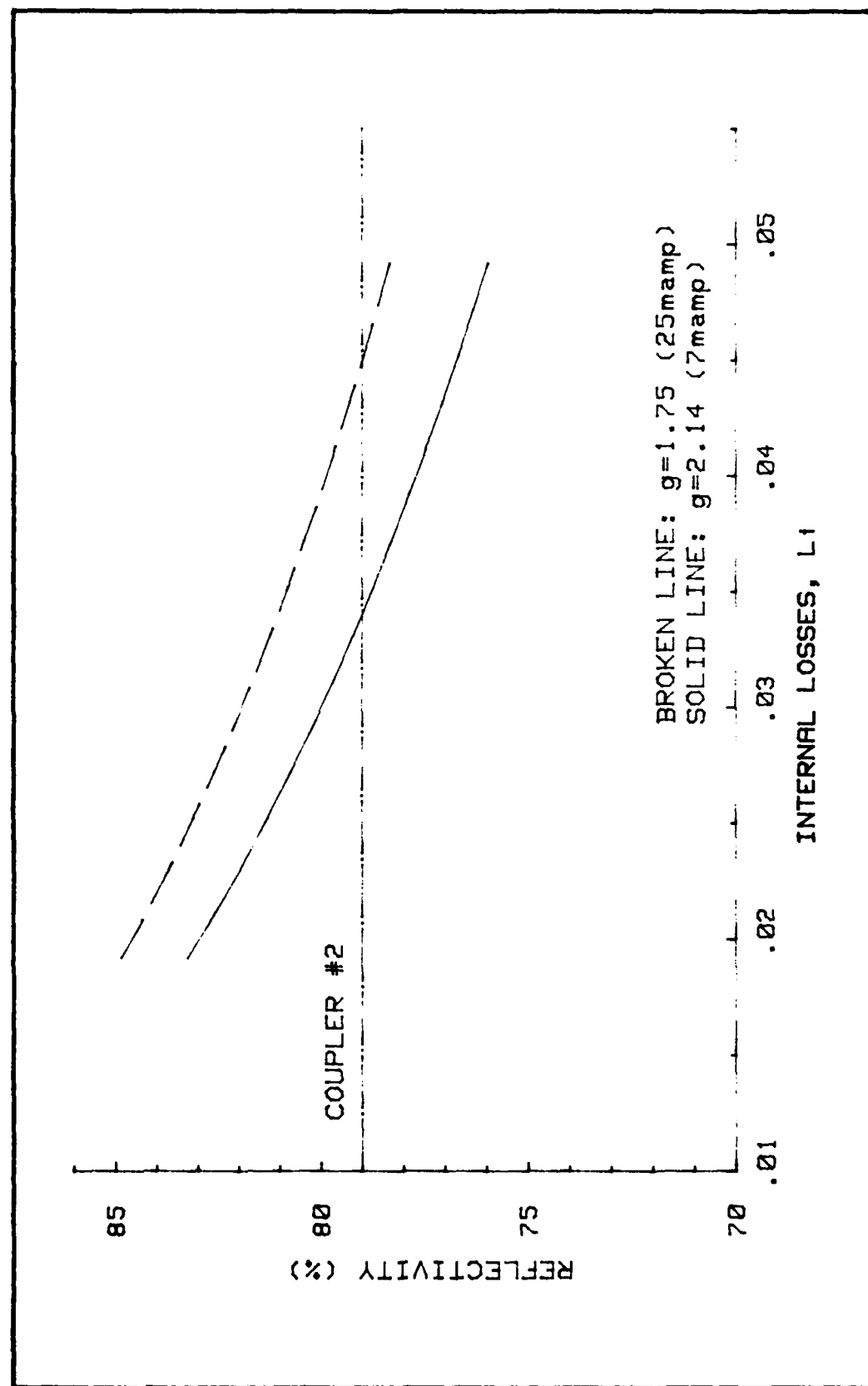
Figure 29. Optimum Reflectivity vs Internal Loss, Li, for 7 mamps and 25 mamps of Current per Anode

VI RECOMMENDATIONS

Unless maximum power is required, the laser should be operated at 9 mamps with 9% Xe at 4.5 torr.

If maximum power is required, 10% Xe at 4 torr with 27 mamps of current should be used. However, external cooling will be necessary for use in excess of about 1½ minutes.

Since the output was susceptibe to temperature changes, an investigation of temperature dependence might be undertaken.

Operate the laser with coupler #2 (R=79.0%). From figure 30, it is apparent that internal mirrors or a mirror closer to the specific optimum value would not be cost efficient.

A thorough investigation of the NEC mode should be made by varying one of the anode currents while maintaining the others constant. This procedure should be accomplished above the current at which the symmetric mode saturates. It should also be accomplished above the current at which the asymmetric mode saturates (e.g. 20% Xe at 8 torr above 24 mamps) to ascertain whether the NEC mode also enhances the asymmetric mode of operation.
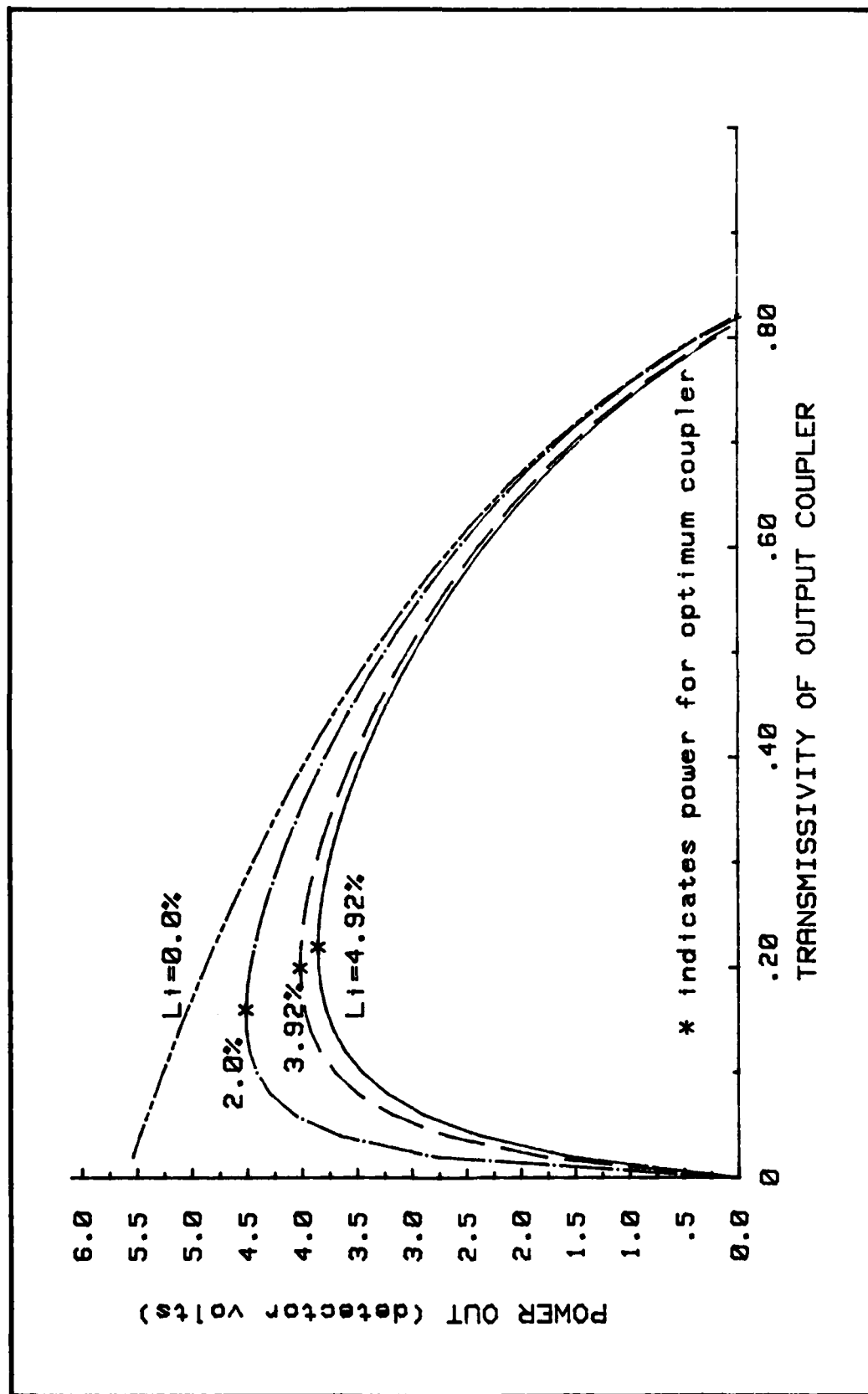
Figure 30. Theoretical Power Out vs Output Transmittance for 25 mamps of Current and Various Internal Losses

BIBLIOGRAPHY

1. Birnbaum, George. <u>Optical Masers</u>. New York: Academic Press, 1964.

2. Bloom, A.L. <u>Gas Lasers</u>. New York: John Wiley and Sons, Inc., 1968.

3. Borodin, V.S., Yu.M. Kagan, and R.I. Lyagushchenko. "Investigation of a Hollow-Cathode Discharge II," <u>Soviet Physics-Technical Physics</u>, <u>11</u>: 887-888 (January 1967).

4. Crane J.K. and H.T. Verdeyen, "The Hollow Cathode Helium-Fluorine Laser," <u>Journal of Applied Physics 51</u> (1): 123-129 (January 1980).

5. DeJoseph, Charles A. Jr. AF Wright Aeronautical Laboratories, Energy Conversion Branch (personal interview). 30 June 1982.

6. Heavens, O.S. <u>Optical Masers</u>. New York: John Wiley and Sons, Inc., 1965.

7. Lengyel, B.A. <u>Introduction to Laser Physics</u>. New York: John Wiley and Sons, Inc., 1966.

8. Olson, Robert A. and Dennis F. Grosjean. <u>Closed-Cycle Rare-Gas Electrical-Discharge Laser</u>. AFAPL-TR-77-13. Wright-Patterson AFB, Ohio: Air Force Aero Propulson Laboratory, April 1977.

9. Paananen, R.A. and D.L. Bobroff. "Very High Gain Gaseous (Xe-HE) Optical Maser at 3.5 µ," Applied Physics <u>Letters</u>, <u>2</u>: 99-101 (1 March 1963).

10. Papoular, R. <u>Electrical Phenomena in Gases</u>. New York: American Elsevier Publishing Company, Inc., 1965.

11. Patek, Karel. <u>Lasers</u>. Cleveland: CRC Press, 1967.

12. Pedrotti, Leno S. and Hugo Weichel. Lecture materials distributed in PH 7.43, Laser Physics I. School of Engineering, Air Force Institute of Technology, Wright-Patterson Air Force Base, Ohio, 1982.

13. Penning, F.M. <u>Electrical Discharges in Gases</u>. Holland: N.V. Philips; Gloeilampenfabrieken, 1957.

14. Racah, G. "On a New Type of Vector Coupling in Complex Spectra," <u>Physical Review</u>, <u>61</u>: 537 (April 1 and 15, 1942).

15. Ross, Dieter. <u>Lasers Light Amplifiers and Oscillators</u>. New York: Academic Press, 1969.

16. Sturges, D.J. and H.J. Oskam. "A Qualitative Theory of the Medium Pressure Hollow Cathode Effect," Physica, 37: 460-461 (1967).

17. Vogel, George A. Analysis of XeCl Emission in a Hollow Cathode Discharge. MS thesis. Wright-Patterson AFB, Ohio: Air Force Institute of Technology, December, 1981.

18. von Engel, A. Ionized Gases. London: Oxford University Press, 1965.

19. Winegarden, Jerry D. Measurement of Cl_2 Concentration in a XeCl Hollow Cathode Discharge Including the Effect of H_2 Addition. MS thesis. Wright-Patterson AFB, Ohio: Air Force Institute of Technology, December, 1980.

20. Wolfe, W.L. and G.J. Zissis. The Infrared Handbook. Washington: Office of Naval Research, 1978.

21. Yariv, Amnon. Introduction to Optical Electronics. New York: Holt, Rinehart and Winston, 1976.

VITA

Jimmy C. Mann was born on 4 January 1949 in Fort Worth, Texas. He is the son of Mr. & Mrs. Eugene A. Mann. He graduated from Eastern Hills High School, Fort Worth, Texas in June 1967 and received a B.S. degree in Mathematics from the University of Texas at Arlington in 1972. He entered the Air Force in October 1973 and graduated from pilot training in April 1975. He was a B-52 pilot for 6 years at Seymour Johnson AFB, North Carolina before entering the Air Force Institute of Technology in June 1981. He was married to Virginia Alongis on 11 September 1980.

Permanent address: 34 Brent St.
                               Chattahoochee, FL.
                                  32324

REPORT DOCUMENTATION PAGE		READ INSTRUCTIONS BEFORE COMPLETING FORM
1. REPORT NUMBER AFIT/GEP/PH/82D-18	2. GOVT ACCESSION NO. AD-A124 768	3. RECIPIENT'S CATALOG NUMBER
4. TITLE (and Subtitle) OPTIMIZATION OF A HELIUM XENON HOLLOW CATHODE DISCHARGE LASER		5. TYPE OF REPORT & PERIOD COVERED MS Thesis
		6. PERFORMING ORG. REPORT NUMBER
7. AUTHOR(s) Jimmy C. Mann Capt		8. CONTRACT OR GRANT NUMBER(s)
9. PERFORMING ORGANIZATION NAME AND ADDRESS Air Force Institute of Technology (AFIT-EN) Wright-Patterson Air Force Base, Ohio 45433		10. PROGRAM ELEMENT, PROJECT, TASK AREA & WORK UNIT NUMBERS
11. CONTROLLING OFFICE NAME AND ADDRESS		12. REPORT DATE December 1982
		13. NUMBER OF PAGES 78
14. MONITORING AGENCY NAME & ADDRESS(if different from Controlling Office)		15. SECURITY CLASS. (of this report) Unclassified
		15a. DECLASSIFICATION/DOWNGRADING SCHEDULE

16. DISTRIBUTION STATEMENT (of this Report)

Approved for public release; distribution unlimited

17. DISTRIBUTION STATEMENT (of the abstract entered in Block 20, if different from Report)

18. SUPPLEMENTARY NOTES

Approved for public release: IAW AFR 190-17.   Approved for public release; IAW AFR 190-17

LYNN E. WOLAVER
Dean for Research and Professional Development   FREDRIC C. LYNCH, Major, USAF   6 JAN 1983
Air Force Institute of Technology (AIC)   Director, Public Affairs
Wright-Patterson AFB OH 45433

19. KEY WORDS (Continue on reverse side if necessary and identify by block number)

He-Xe
Xe
Hollow Cathode Discharge
Laser
Hollow Cathode Discharge Laser

20. ABSTRACT (Continue on reverse side if necessary and identify by block number)

This work investigates the characteristics of a fixed geometry hollow cathode discharge laser containing various pressures and mixtures of helium (He) and xenon (Xe). The laser oscillates at an infrared wavelength of 3.507 microns. Power from three output couplers using mixtures of 2.5% to 20% Xe at pressures of two to eight torr are investigated. The output power is measured as a function of mixture, pressure, and output coupler.

DD FORM 1473   EDITION OF 1 NOV 65 IS OBSOLETE
1 JAN 73

A "modes of operation" model is developed to explain the variations in the curves for power vs anode current. The symmetric mode of operation is characterized by equivalent voltages driving the three anodes at the same current. The asymmetric mode of operation is characterized by the same currents being driven by different voltages, hence the asymmetry. The non-equal current (NEC) mode of operation is characterized by at least one of the anodes being driven at a different current.

The results of the investigation reveal a maximum power of 1.16 mw with 10% Xe at 4 torr of pressure with an anode current of 27 mamps. Evidence is also presented that the asymmetric and NEC modes of operation can provide additional power after the symmetric mode has saturated.

END

FILMED

3-83

DTIC